J. Fluid Mech. (1985), *vol.* 155, *pp.* 465–510
Printed in Great Britain

The hydrodynamic stability of flow over Kramer-type compliant surfaces. Part 1. Tollmien–Schlichting instabilities

By P. W. CARPENTER
Department of Engineering Science, University of Exeter, Exeter, England

AND A. D. GARRAD
Garrad Hassan and Partners, 10 Northampton Square, London, EC1M 5PQ, England

The hydrodynamic stability of flows over Kramer-type compliant surfaces is studied. Two main types of instability are considered. First, there are those which could not exist without viscosity, termed Tollmien–Schlichting Type Instabilities (TSI). Secondly, there are Flow-Induced Surface Instabilities (FISI), that depend fundamentally on surface flexibility and could exist with an inviscid fluid flow. Part 1, the present paper, deals mainly with the first type. The original Kramer experiments and the various subsequent attempts to confirm his results are reviewed, together with experimental studies of transition in flows over compliant surfaces and theoretical work concerned with the hydrodynamic stability of such flows.

The Kramer-type compliant surface is assumed to be an elastic plate supported by springs which are modelled by an elastic foundation. It is also assumed that the plate is backed by a viscous fluid substrate having, in general, a density and viscosity different from the mainstream fluid. The motion of the substrate fluid is assumed to be unaffected by the presence of the springs and is determined by solving the linearized Navier–Stokes equations. The visco-elastic properties of the plate and springs are taken into account approximately by using a complex elastic modulus which leads to complex flexural rigidity and spring stiffness. Values for the various parameters characterizing the surface properties are estimated for the actual Kramer coatings.

The boundary-layer stability problem for a flexible surface is formulated in a similar way to that of Landahl (1962) whereby the boundary condition at the surface is expressed in terms of an equality between the surface and boundary-layer admittances. This form of the boundary condition is exploited to develop an approximate theory which determines whether a particular change to the mechanical properties of the surface will be stabilizing or destabilizing with respect to the TSI. It is shown that a reduction in flexural rigidity and spring stiffness, an increase in plate mass, and the presence of an inviscid fluid substrate are all stabilizing, whereas viscous and visco-elastic damping are destabilizing.

Numerical solutions to the Orr–Sommerfeld equation are also obtained. Apart from Kramer-type compliant surfaces, solutions are also presented for the rigid wall, for the spring-backed tensioned membrane with damping, previously considered by Landahl & Kaplan (1965), and for some of the compliant surfaces investigated experimentally by Babenko and his colleagues. The results for the Kramer-type compliant surfaces on the whole confirm the predictions of the simple theory. For a free-stream speed of 18 m/s the introduction of a viscous substrate leads to a complex modal interaction between the TSI and FISI. A single combined unstable

mode is formed in the case of highly viscous substrate fluids and in this case increased damping has a stabilizing effect. When the free-stream speed is reduced to 15 m/s the modal interaction no longer occurs. In this case the effects of combined viscous and visco-elastic damping are investigated. It is found that damping tends to have a strong stabilizing effect on the FISI, in the form of travelling-wave flutter, but a weaker destabilizing effect on the TSI. The opposing effects of damping on the two modes of instability forms the basis of a possible explanation for Kramer's empirical observation of an optimum substrate viscosity. Results obtained using the e^9 method also indicate that a substantial transition delay is theoretically possible for flows over Kramer's compliant coatings.

1. Introduction

More than twenty-five years have passed since Kramer (1957, 1960*a*) first described his pioneering experiments on compliant coatings. Nevertheless, despite much work by subsequent investigators, both theoretical and experimental, apparently no independent evidence has been obtained for the drag-reducing capabilities of Kramer's coatings. Indeed, in many such tests, similar coatings have actually yielded higher drags than comparable rigid surfaces. It is probably no exaggeration to suggest that the credibility of Kramer's coatings is now rather low. Certainly, current research has been focused on rather different sorts of compliant surfaces.

In our opinion, however, the case against Kramer's coatings may not be so strong as popularly supposed. Kramer himself believed that the drag reductions achieved in his tests were a result of the transition-delaying properties of his coatings. At present there is no hard evidence to support this view. On the other hand, it is also true, as we will seek to show below, that the independent tests carried out on the Kramer coatings were completely unsuitable for investigating transition. It also appears that hitherto no reasonably complete theoretical study has been undertaken of the hydrodynamic stability of flows over Kramer-type surfaces in order to see whether there is any theoretical basis for Kramer's views. The main objective of the present paper is to describe such a study. Much of the analysis and many of the results should have a wider application, however.

It is also possible, of course, that the drag reductions observed by Kramer were a result of the compliant surface interacting in some way with a fully developed turbulent boundary layer. It could be argued that this would be a more fruitful line of inquiry than a study of the transition process. After all it has been established experimentally (see Walters & Blick 1968; Blick *et al.* 1969; Grosskreutz 1971, 1975; Loof 1974; and Fischer *et al.* 1975) that turbulence levels can be reduced in boundary layers over certain compliant surfaces. Nevertheless, in our opinion, there is little prospect in the near future of achieving any sort of real understanding of the influence of compliant surfaces on turbulent boundary layers. On the other hand it seems to us that very considerable progress could be made towards an increased understanding of the transition process simply by adapting and extending existing techniques. By and large this is the course we have followed in the present paper by applying linear hydrodynamic stability theory to compliant surfaces.

Benjamin (1960) has shown that the transition process over flexible surfaces is complicated by the appearance of additional modes of instability. For a passive surface there are two broad categories of instabilities. First, there are those instabilities which could not exist without viscosity. These we will call Tollmien–Schlichting Type Instabilities (hereinafter referred to as TSI). They can be radically

affected by the induced surface motion but remain essentially similar to those in the boundary layer over a rigid surface. These instabilities are the subject of Part 1, the present paper. Second, there are the instabilities which depend fundamentally on surface flexibility and could exist with an inviscid fluid flow. These we will call Flow-Induced Surface Instabilities (hereinafter referred to as FISI). On the whole they are similar to the instabilities encountered in aeroelasticity. Part 2 will be devoted to these instabilities.

It could be argued that the categorization of the types of instability, proposed in the previous paragraph, is rather artificial. After all, both the TSI and FISI in the form of travelling-wave flutter are eigenvalues of the system comprising the Orr–Sommerfeld equation coupled with the equation of motion for the compliant surface. In fact, when the compliant surface is dissipative a complex interaction may occur† between these two modes of instability. Insofar as they can be obtained numerically as eigenvalues of the coupled Orr–Sommerfeld/surface equations, the FISI are investigated in Part 1, the present paper. However, a purely inviscid theory can be developed for the FISI and such a theory will be presented in Part 2. Not only are many additional features of the FISI elucidated by this inviscid theory but, in addition, its results are required in order to obtain the present numerical solutions for the travelling-wave flutter form of the FISI. Moreover, some modes of the FISI, such as static divergence, cannot be investigated by means of numerical integration of the Orr–Sommerfeld equation.

Section 2 of this paper contains a review of previous work, subdivided into §2.1 which describes Kramer's experimental investigations, §2.2 which reviews other relevant experimental work, and §2.3 which reviews the literature concerned with stability analyses of boundary layers over compliant surfaces. Section 3 describes the theoretical model for Kramer-type compliant coatings and the evaluation of the parameters characterizing the Kramer coatings. The boundary-layer stability problem for a flexible surface is formulated in §4. An approximate theory for TSI on flexible surfaces is developed in §5. The numerical methods used for the present work are described in §6. The results of the numerical analysis are presented and discussed in §7. Results for a rigid flat plate are given in §7.1. In §7.2 a comparison is made between Landahl & Kaplan's (1965) and our results for a spring-backed membrane. A comparison is also made in §7.3 between the results of the present theory and of an experimental investigation into hydrodynamic stability of flow over flexible surfaces carried out by Babenko and his colleagues. Lastly, in §7.4, the Kramer coatings are investigated. Section 8 contains the conclusions drawn from the present study of TSI in flows over compliant surfaces.

2. Review of previous work

2.1. *Kramer's experimental investigations*

The first type of compliant surface designed by Kramer (1957, 1960*a*) is shown in figure 1 (*a*, *b*). An inner rigid wall was covered by a flexible inner skin which was connected to a fairly thick (2 mm) outer flexible diaphragm by a closely spaced array of stubs. The flexible inner skin, outer diaphragm and stubs were all made of the same soft natural rubber. The cavity between the outer diaphragm and inner skin was filled with a highly viscous damping fluid. In Kramer's view the function of this fluid was to damp out 'boundary-layer' waves (presumably he was referring to TSI). The

† A complete analysis of these interactions will be presented in Part 3.

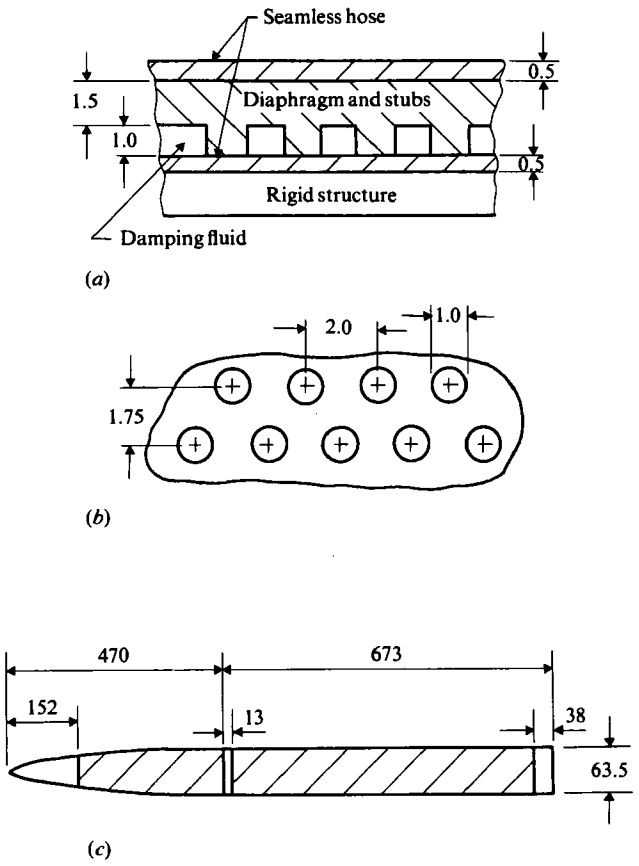

FIGURE 1. Kramer's coating and model. All dimensions in mm. (Drawings based on those given by Kramer 1960*a*.) (*a*) Cross-section. (*b*) Cut through stubs. (*c*) Model: shaded regions were coated.

damping mechanism was assumed to involve an interaction between the fluid motion in the cavity and the stubs. Accordingly, the spacing between the stubs was chosen to be about one-quarter of the critical wavelength at the design speed. Kramer also considered that if the stiffness and inherent damping of the heavy outer diaphragm were properly chosen then it could act as distributed damping and thereby reduce the detrimental effects of the local turbulent disturbances which have a much higher frequency than TSI. Thus the coating was regarded as consisting of two wide-frequency-band dampers.

Kramer (1960*b*) apparently studied the mechanical properties of dolphin skin fairly closely before designing the compliant coating depicted in figure 1 (*a*, *b*). Certainly, from photographs of sections through dolphin skin presented by Kramer (1960*b*, 1965) it appears that his coatings bear a considerable resemblance to dolphin skin. According to Babenko, Gintetskii & Kozlov (1969) and Babenko, Kozlov & Pershin (1972), however, Kramer's photographs are misleading and, in fact, his coatings would not function in the same way as dolphin skin. A simplified diagram of a section through a typical portion of dolphin skin is shown in figure 2, which is based on figure 115 of Aleev (1977). The upper epidermal layer forms a comparatively dense elastic membrane and is thought capable of transmitting without distortion all boundary-layer pressure fluctuations to the underlying layer of the epidermis. This

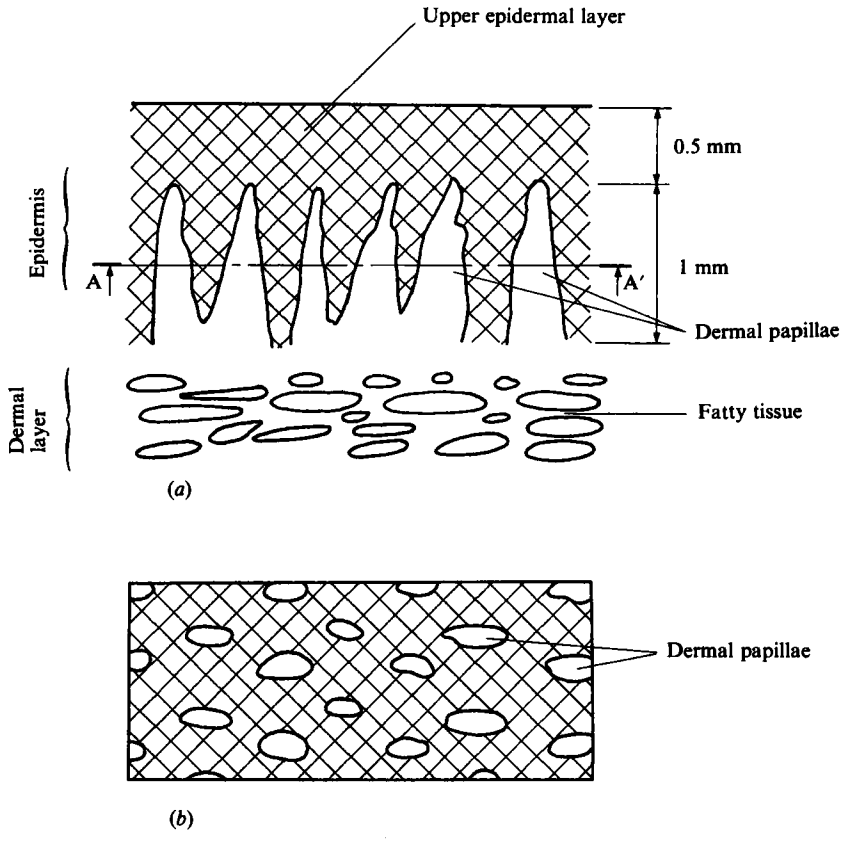

FIGURE 2. Structure of dolphin skin (based on photographs given in figure 115 of Aleev 1977). (*a*) Cross-section. (*b*) Cut through dermal papillae at AA'.

layer and the dermal papillae are made of looser, more hydrated tissue including fat cells. Thus, unlike the stubs in Kramer's coatings, the papillae in dolphin skin are actually more readily deformable than their surroundings. Babenko *et al.* also claim that the blood flow through the dermal papillae can be regulated thereby allowing the viscoelastic properties of the papillary layers of the dermis and the skin as a whole to be altered by the nervous system. This would mean that dolphin skin is subject to a certain amount of active control, unlike Kramer's purely passive coatings.

Kramer's coatings may not have functioned like dolphin skin but, nevertheless, his test results showed that very considerable drag reductions could be achieved with them. Some preliminary test results were reported by Kramer (1957). These were promising, so further tests were carried out under more carefully controlled conditions. These tests and their results are described by Kramer (1960*a*). The coated model used for these tests is depicted in figure 1(*c*). It was a streamlined body of revolution consisting of a 470 mm long tip having a tabulated contour followed by a cylindrical aft section 673 mm in length and 63.5 mm in diameter. The first 152 mm of the tip, a 13 mm transition section between the tip and the cylinder and the last 38 mm of the cylinder were not covered with compliant coating. The model was sling-mounted to an after-body and the whole was towed in the sea at speeds up to 18 m/s. The ambient turbulence level was less than 0.1 % at the time of the tests although it varied considerably with the time of year (Kramer 1962, 1965).

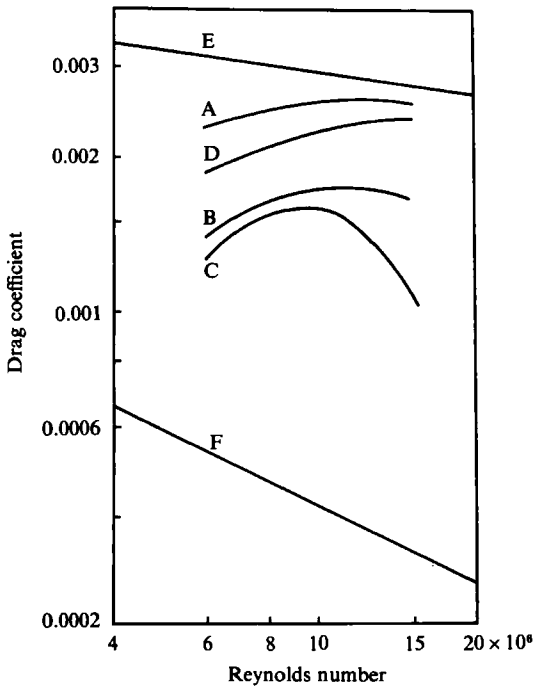

FIGURE 3. The drag coefficient of various Kramer coatings as a function of Reynolds number. Curve A: The rigid reference model. Curves B, C, D: Coated models, coating stiffnesses: B, 0.434 N mm^{-3}; C, 0.217 N mm^{-3}; D, 0.167 N mm^{-3}. Curve E: Fully turbulent flow. Curve F: Fully laminar flow.

Three different rubbers were used, giving coatings with three different grades of stiffness. Several different damping fluids having a wide range of kinematic viscosities were also tested. Kramer's (1960*a*) results are displayed in figure 3 as drag coefficients plotted against Reynolds number. It can be seen that the coating having intermediate stiffness performed best, with a drag reduction of almost 60 % at the highest Reynolds number. Kramer also found that a 300 cSt damping fluid gave the best results for this coating.

It was found subsequently that the coatings tended to deteriorate with the passing of time and then yielded inferior results. Consequently Kramer (1962) designed and tested a more robust type of coating. With this new design the stubs were replaced by longitudinal ribs aligned in the flow direction. These new coatings performed slightly less well than freshly made coatings of the original design, but nevertheless still possessed a very considerable drag-reduction capability.

2.2. *Other experimental work*

On the whole, the comments made below will be confined to experimental studies of Kramer-type coatings and of transition on any sort of compliant surface. A much more comprehensive review of the experimental work with compliant surfaces is given by Bushnell & Hefner (1977). There are also the more specialized reviews by Dinkelacker (1977) and de Loof (1974), who mostly deal, respectively, with work at the Max-Planck-Institut für Strömungsforschung, Göttingen, and at Bertin et Cie, France.

Before reviewing the attempts made to confirm Kramer's results it is worth briefly considering what requirements should be met by such experimental investigations

in order to make a favourable outcome likely. First, let us consider the coating itself. Kramer's results in figure 3 suggest that the value of the coating stiffness is fairly critical. A coating performs much less well if it is less or more stiff than the optimum value. Our own theoretical results bear this out. In Part 2 (some preliminary results are given by Garrad & Carpenter 1982; Carpenter & Garrad 1982; and Carpenter 1984*b*) we find that the best coating (C) is marginally unstable with respect to FISI at the top test speed, while the softest coating (D) appears to be much more unstable. On the other hand our theoretical results in §7 of this paper show that the hardest coating (B) is much less efficient at reducing the growth rate of TSI. Our results also indicate that viscoelastic damping may have a strong influence on the FISI. From these considerations it can be concluded that a successful coating should be as similar as possible to Kramer's best coating both with respect to configuration and materials. Kramer also indicated that there is an optimum value for the viscosity of the damping fluid. This is borne out to a limited extent by our results. In §7 it is shown that an increase in viscosity may impair the coatings' capacity to reduce the growth rate of the TSI. On the other hand it is shown that an increase in viscosity leads to a reduction in the growth rate of the FISI.

Let us now consider the design of the test model itself. Kramer apparently designed his model (see figure 1*c*) with some care. It would be expected that over most of the body the pressure gradient would be favourable or close to zero. This in itself is conducive to the maintenance of laminar flow. To judge from our results in §7, Kramer's coatings are only marginally capable of delaying transition. Therefore, any unfavourable factor, such as an adverse pressure gradient or lack of smoothness where the compliant surface is joined to a rigid surface, could badly affect the coating's performance. Similar considerations would imply that conventional water tunnels, with their relatively high free-stream turbulence levels, would be unsuitable for such tests. Lastly, it should be noted that Kramer's coatings were designed for a relatively restricted Reynolds-number range and are unlikely to perform well outside this range.

At least four attempts have been made to carry out tests in order to provide independent verification of Kramer's results. These are reported by Puryear (1962), Nisewanger (1964), Ritter & Messum (1964) and Ritter & Porteous (1965). No significant drag reduction was observed in any of the four sets of tests. Each investigation will now be briefly considered to see whether or not it met the requirements set out above for a successful test.

Puryear's (1962) experiments were carried out in a towing tank at speeds up to 20.5 m/s. He used a coating similar to Kramer's. He did not specify explicitly the elastic modulus of the rubber but used the term 'high modulus' to describe it, which suggests his coating is likely to be most similar to Kramer's stiffest coating. The models were modified prolate spheroids 2.495 m long with a maximum diameter of 325 mm; 2.175 m of the total length was covered with the coating, which was filled with a 1000 cSt solution of polyethylene oxide (polyox) and water. FISI in the form of wrinkles were observed at speeds exceeding 18 m/s. The models covered with compliant coatings had 2–6 % more drag than the rigid ones. Puryear attributed these disappointing results to problems encountered in making a smooth join between the rigid nose and the coating. Apparently cavitation and separation frequently occurred at the leading edge of the coating. It also appears that the coating being tested was not equivalent to the Kramer coating with the best performance.

The models tested by Nisewanger (1964) were bodies of revolution 3.63 m long in total, with compliant coating covering the first metre. The noses of the models were made of rubber and were blunt, rather than streamlined. The coatings were reported

to be of Kramer 'Lamiflo' type, but the coating stiffness was not given. Water and polyethylene oxide were used as damping fluids; the latter has a viscosity of 2000 cSt. Thus it is clear that Kramer's optimum value for viscosity was not tested. The test vehicle was towed to the bottom of a lake and released, whereupon it was propelled upwards by its own buoyancy. Speeds of up to 20 m/s were achieved. The results were not very consistent, but it appears that the drag of the coated bodies was about 6% more than for the rigid body when filled with water, and about 11% more with polyethylene oxide. FISI were observed at speeds greater than 18 m/s in preliminary tests in a towing tank. It seems highly probable that the blunt nose of the model would give rise to an unfavourable pressure gradient over much of the compliant coating. So it is perhaps to be expected that this test would be unsuccessful, especially since again the coatings being tested were not equivalent to Kramer's best coating.

Ritter & Messum (1964) carried out their tests on 305 mm square flat-plate models covered with compliant coating. A small flat plate is not really comparable to Kramer's original model so it was, perhaps, not altogether surprising that no significant drag reduction was observed. The work was continued by Ritter & Porteous (1965), who used a more satisfactory model. The new model was a 4.215 m long cylindrical model of 208 mm diameter having an elliptical nose. The tests were carried out in a water tunnel having a 762 mm wide working section. The nose was fitted to the leading edge of the coated cylinder in such a way that the boundary layer could be removed by suction through a slot between the nose and cylinder. This arrangement ensured that there was laminar flow at the start of the coated cylinder. The coatings tested were selected by Kramer's collaborators at the Research Laboratory of the U.S. Rubber Co. It is not clear what stiffness the coatings had, compared to Kramer's original coatings. However, Ritter & Porteous state that there was a choice of two stiffnesses and they chose the softer rubber. They also reported the occurrence of FISI in the form of blisters and humps when the speed exceeded 14 m/s. Consequently, most tests were carried out at 12 m/s. From a comparison with our theoretical results to be presented in Part 2 (see also Garrad & Carpenter 1982 and Carpenter & Garrad 1982) these observations suggest that they were using a coating equivalent to Kramer's softest coating (D). If so, the fact that their coatings failed to yield any significant drag reduction is quite understandable. Also it is unlikely that the turbulence levels in a water tunnel would be low enough to maintain laminar flow far beyond the suction slot at the join between the nose and the coating. Another factor, which possibly had an adverse effect, was the use of water as the damping fluid for most of the tests. It must be admitted, though, that the performance of Kramer's coating (D) did not appear to depend significantly on the viscosity of the damping fluid in Kramer's (1960*a*) original tests. Ritter & Porteous also experienced trouble with the leading edge of the coating on their models.

From this brief review of the attempts to corroborate Kramer's original results it can be concluded that the Kramer coatings have not yet been subjected to a satisfactory independent test. The tests described above certainly should not be taken as conclusive evidence that the Kramer coatings are not capable of delaying transition under favourable conditions.

The possibility still remains, of course, that Kramer's observed drag reductions could have been a result of a favourable interaction between the compliant surface and a fully turbulent boundary layer. Two additional explanations† have also been

† The authors are indebted to one of the referees for bringing these explanations to their attention.

suggested for Kramer's results. First, the drag reductions could have come about owing to favourable changes to the pressure drag. These could conceivably have occurred owing to surface discontinuities at the coated–uncoated interfaces and/or to a favourable modification of the flow near the rear of the body leading to lower base drag. Secondly, there is a possibility that drag-reducing polymeric material, e.g. the silicone oil used as the damping fluid, was exuded by the surfaces during the tests. If this were the sole explanation, however, it is hard to see why Kramer's stiffest coating (B) should have had a higher drag than the coating (C) with intermediate stiffness.

Before turning to the work on transition, mention should be made of the compliant coating tested by Grosskreutz (1971, 1975). This coating can be regarded as an extension of the original Kramer design. Grosskreutz's aim was to design a compliant surface which moved in such a way that the product of its normal and longitudinal velocities would be positive for all or most of the time. It might be expected that the Reynolds shear stress, and therefore turbulence production (or, for that matter, the growth of small disturbances in a laminar boundary layer), would be considerably reduced near the surface. This idea also follows from Ffowcs Williams' (1964) analysis of the Reynolds shear stress near a flexible surface. Grosskreutz's coatings were quite similar to Kramer's, except that the stubs were inclined at 45° into the flow direction.† The coatings were made of silicone rubber. The models were of flat-plate type, measuring 800×248 mm; the coatings covered 650×204 mm of the surface. Tests were carried out in a water tunnel at speeds up to 7 m/s. The best coating yielded a 3.6% reduction in momentum thickness at 1.5 m/s but a considerable increase occurred for speeds greater than 2.3 m/s. More discouraging, as far as confirming the basic concept is concerned, is the fact that the coating performed almost as well when the direction of inclination of the blades was reversed. Like Kramer, Grosskreutz also found that any favourable effects disappeared when the coatings aged.

Let us now consider experimental observations of the transition process in boundary layers over compliant surfaces. There appears to be little information available on this subject. Karplus (1963) described experiments with water flowing over polyester (mylar) film stretched over various damping fluids. His results are different to interpret but appear to show that compared to rigid surfaces small disturbances become unstable earlier for flexible walls but their growth rate is lower. Mattout (1972) carried out an experimental investigation of compliant surfaces consisting of polyvinyl chloride (PVC) and polyester (mylar) films stretched over polyurethane foam. The models were of flat-plate type and were tested in a water tunnel. The reported variation of turbulence intensity in the streamwise direction indicated that transition sometimes occurred slightly earlier or later for the flexible surfaces compared to the rigid control.

A very thorough experimental investigation of the hydrodynamic stability of boundary layers over flexible surfaces has been carried out by Babenko and his colleagues at the Institute of Hydromechanics, Kiev, in the Soviet Union. The apparatus and methodology were described by Babenko, Gintetskii & Kozlov (1972). The experiments were carried out in a low-turbulence (less than 0.05% turbulence intensity) water flow at speeds between 0.05 to 0.15 m/s. The growth of small disturbances, which were generated at controlled frequencies, was detected by means

† It is interesting to note that according to Babenko & Surkina (1964) the dermal papillae of dolphin skin are inclined at angles to the flow direction ranging from 15°–80°.

of the tellurium technique developed by Wortmann (1953, 1969). The experimentally determined neutral-stability boundaries for a rigid wall presented by Babenko & Kozlov (1973) agree reasonably well with those of Schubauer & Skramstadt (1948) and Ross *et al.* (1970). This confirms that their methods were basically sound. The compliant surfaces consisted of either a polyvinyl-chloride (PVC) membrane stretched over a cavity filled with water or a cavity containing polyurethane foam with or without a polyethylene film stretched over it. The experimental methods used to determine the mechanical properties of the compliant surfaces are described by Babenko (1973*b*). The results for the simple membrane surfaces are given by Babenko (1973*a*) and those for foam with or without membranes in Babenko & Kozlov (1973). The best results were obtained with a flat strip of polyurethane foam without a tensioned membrane. In this case the critical Reynolds number was approximately doubled and the amplification rate halved, compared to the rigid wall. The addition of a tensioned membrane increased the region of instability compared to the rigid wall. For the simple membrane surfaces, Babenko found that the critical Reynolds number was not greatly different from the rigid-wall value, but an increase in cavity depth and membrane tension tended to increase the region of instability.

Owing to the well-documented information on the surfaces we were able to use our theoretical methods to predict the neutral curves for some of Babenko's simple membrane surfaces. The results are shown in figure 10 and discussed in §7.3. The theoretical neutral curves for Babenko's flexible surfaces are almost indistinguishable from those corresponding to a rigid wall. It must be pointed out, however, that, for the values of Reynolds numbers involved, the neutral curve for the rigid wall obtained using linear stability theory bears little resemblance to the experimental results. It is also true, of course, that this part of the neutral curve is not really relevant to the transition process, which involves small disturbances of considerably longer wavelengths at higher Reynolds numbers. So for this reason Babenko and his colleagues have not really provided any direct information on the *transition* process over compliant surfaces.

2.3. *Stability analyses of boundary layers over compliant surfaces*

We will confine ourselves to reviewing the literature concerned with linear stability analyses of boundary layers over compliant surfaces. A more extensive review covering some of the same ground was given by Richards (1968), while a far more wide-ranging discussion of related topics can be found in an excellent review by Benjamin (1964). A very comprehensive review is also given by Bushnell & Hefner (1977) who discuss theoretical analyses of turbulent boundary layers on compliant surfaces as well as stability analyses and other topics.

The effects of a flexible boundary on hydrodynamic stability were first studied in depth by Benjamin (1960) who provided the foundations for much of the subsequent work. He pointed out that the motion of the flexible surface would be likely to change radically the thin friction layer at the wall. Since the destabilizing action of viscosity on TSI is generated in this friction layer, then surface flexibility could very well have a favourable effect on boundary-layer stability.

Benjamin showed how the boundary conditions at the wall could be formulated for the case of a flexible surface with predominantly normal motion. (This is by no means a trivial step since some subsequent investigators have used an incorrect form of the no-slip condition.) The response of the flexible surface to the pressure generated by the fluid motion was characterized by introducing a response coefficient (a complex compliance) Z which corresponds to the surface deflection due to a pressure wave of unit amplitude.

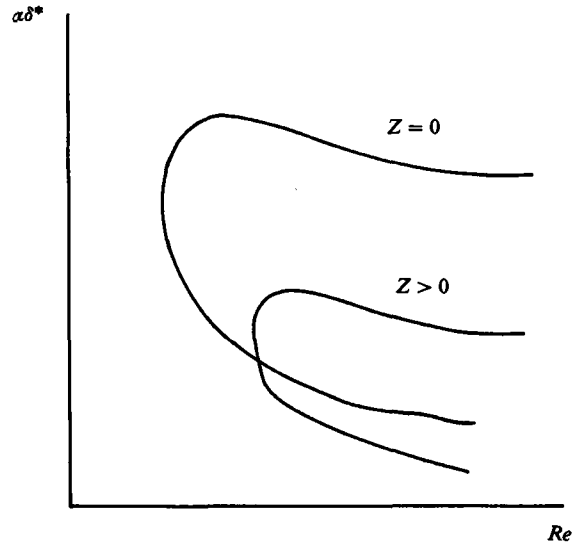

FIGURE 4. The effect of surface compliance on the neutral curve for a non-dissipative flexible wall according to Benjamin's theory: α is wavenumber; δ^* is boundary-layer displacement thickness; and Re is Reynolds number based on δ^*.

By means of an ingenious, but remarkably simple, extension of the conventional linear stability theory of Tollmien (1929), Schlichting (1933) and Lin (1945), Benjamin was able to show how a flexible non-dissipative wall will tend to stabilize TSI which have phase velocities lower than c_0, the velocity of free waves on the surface. When $Z_r > 0$† the neutral curves are shifted to lower wavenumbers and higher Reynolds number, as shown in figure 4. In the case of dissipative flexible walls he showed that internal damping destabilizes TSI. A similar conclusion was independently reached by Betchov (1960) (see also Betchov & Criminale 1967).

Benjamin also pointed out that for flow over flexible surfaces other modes of instability could be excited in addition to TSI (classified as Class A waves). The additional instabilities were surface waves which could occur even with an inviscid fluid flow. Class B was a surface-resonance type of instability and comprised waves travelling at velocities close to the free wave speed of the surface. Class C instabilities were of Kelvin–Helmholtz type, e.g. the flutter instability caused by the coalescence of two modes, which is familiar to aeroelasticians. In the light of Landahl's (1962) analysis the classification scheme was later made more precise by Benjamin (1963), with respect to the surface waves generated by inviscid flows. Further discussion of the flow-induced surface-wave instabilities is postponed until Part 2.

On the basis of his analysis, Benjamin considered that two distinct types of flexible wall may have a significant stabilizing effect on the boundary layer. The first type, which could be called a resonant surface, should be so designed that c_0 is close to the phase speed of the fastest-growing Class A instability. In this case both Class A and B waves would have similar phase speeds and may interact in such a way as to have a favourable effect on the wall friction layer. Kramer's coating was thought to be of this type. The second type, which could be termed a compliant surface, would have to be flexible enough to have a fairly large negative value of Z_r but, at the same time,

† The imaginary part of Z is zero for a non-dissipative wall.

have little internal damping. In this way stabilization of Class A instabilities would be achieved. However, c_0 would have to be large enough to avoid Class B instabilities.

The response of the flexible surface was characterized by Landahl (1962) as an admittance, defined as

$$Y = -\frac{\text{normal wall velocity}}{\text{wall pressure}}.$$

The concept of admittance was borrowed from acoustics. This formulation does not have any real theoretical advantage over that of Benjamin. However, it is also used in the present paper since it is convenient for numerical work. Landahl's theoretical approach makes it possible to determine, relatively simply, whether a particular change in the mechanical properties of the wall will be stabilizing. This feature is exploited in §5. Landahl attempted to simulate in an approximate fashion the principal properties of a Kramer-type coating, and obtained neutral curves numerically. The neutral curves tended to have two branches. He confirmed Benjamin's conclusion with regard to the destabilizing effect of internal damping on TSI (Class A) and considerably clarified matters as regards the effects of damping on the various types of instability. Concerning Kramer's coating he concluded that, since the theoretically predicted critical Reynolds numbers were at best only modestly improved by wall flexibility, it was unlikely that the drag reductions observed by Kramer were a result of delaying transition. The fact that Kramer's best results were obtained with a highly viscous damping fluid was held to be further evidence for this view.

Landahl's theory was used by Gyorgyfalvy (1967) to carry out an extensive parametric study of stability and transition of boundary layers over spring-backed membranes with internal damping. The e^9 method of Smith & Gamberoni (1956) was used to calculate the transitional Reynolds number based on displacement thickness. Gyorgyfalvy found that, when a flexible surface had a favourable effect on transition, it was because of a reduction in amplification rates rather than increase in critical Reynolds number. The potential drag reduction was estimated to be up to 90% in water flows. Large reductions were only available for a comparatively small range of Reynolds numbers, however. Gyorgyfalvy's results appeared to confirm Landahl's views on the theoretical unsuitability of Kramer's coatings for delaying transition.

The formulation of the wall boundary conditions was extended by Landahl & Kaplan (1965) to cases where the surface velocity could have a significant streamwise component, by introducing an additional surface admittance for the streamwise motion. The Orr–Sommerfeld equation was integrated numerically, which allowed accurate solutions to be obtained for a variety of problems. In addition to spring-backed membranes, compliant surfaces formed by a non-dissipative elastic medium (Kaplan 1964)† and by a viscoelastic medium (Voight body) were studied. The effects of pressure gradient on boundary-layer stability over flexible surfaces were also investigated, and the effect of a flexible surface on the secondary instabilities was briefly studied. It was found that a flexible wall would noticeably, but only slightly, reduce the growth rate of the secondary instability. This confirmed a similar conclusion reached by Benjamin (1964) using a simpler flow model. The conclusions reached regarding spring-backed membrane surfaces with internal damping were similar to those mentioned above, reached later by Gyorgyfalvy (1967). It was considered that in order to have a significant favourable effect on transition the use

† Most of the other material in Kaplan (1964) appears in Landahl & Kaplan (1965).

of a light, highly flexible wall would be necessary. Our own calculations (see §7.2) have placed some doubt on Landahl & Kaplan's results for spring-backed membrane surfaces. Their overall conclusions for these surfaces appear to be sound, however.

Some other contributions to hydrodynamic-stability theory for flow over flexible surfaces will now be briefly considered. Nonweiler (1961) investigated flows over non-dissipative elastic walls. Korotkin (1965) developed an alternative formulation of the problem to those of Benjamin, Landahl and Kaplan. His formulation allowed for both normal and tangential compliance but unfortunately the no-slip condition appears to have been incorrectly implemented. Amongst other things Korotkin investigated the effects of a streamwise pressure gradient. Amfilokhiev, Droblenkov & Zavordkhina (1972) used Korotkin's approach to calculate amplification rates and predict transitional Reynolds numbers. Their conclusions were qualitatively in agreement with those of Gyorgyfalvy.

Conventional linear-stability theory has been used for almost all the work reviewed above. Bushnell & Hefner (1977) have questioned the validity of this approach for flows over Kramer-type flexible surfaces. They argued that the modulation produced by such a wall can be sufficient to alter significantly the effective-mean-velocity profile. Accordingly they advocate the use of stability analysis for periodically time-varying mean flows. It seems to us that their argument would only be valid if the wall motion were independent of the instability under consideration. This would clearly be so in the case of active walls. For passive walls, on the other hand, this situation would only arise if the effects of a FISI on TSI were considered. Two main types of behaviour would seem to be possible, i.e. either the two modes of instability would be well separated and distinct or some sort of first-order modal interaction would occur (as in Benjamin's concept of the resonant wall, for example).

In the first case, provided that the amplitudes of the separate instabilities are small enough for linearization to be valid, the instabilities could be treated independently and superposed to give their combined effect. It is certainly possible that any interaction between the two modes of instability could be strongly stabilizing or destabilizing.† However, such an interaction would be a nonlinear higher-order effect. If a first-order interaction occurs leading to the coalescence of the modes, for instance, then clearly the situation is much more complex. However, provided linearization remains valid, there would appear to be no obvious reason why conventional linear theory cannot be used to investigate such interactions. Certainly, it is difficult to see what would be gained by the application of stability analysis for periodic flows.

In summary, then, the current theoretical evidence seems to indicate that it is possible to postpone transition by using a compliant surface but the Kramer coatings are not of a suitable design for this purpose. Moreover, it seems to be firmly established that internal damping destabilizes TSI. So Kramer's explanation for the action of the damping fluid would appear to be incorrect and its true role remains obscure. With regard to these conclusions two points need to be made. First, there has been a tendency in the past to regard the Kramer coatings as spring-backed tensioned membranes. In our view (see the next section) they are better modelled as spring-backed plates with finite bending stiffness. With this sort of model a fairly substantial delay in transition is possible under certain circumstances according to our theoretical results (see §7.4). Secondly, in much of the previous work attention

† It is interesting to note that in a recent study of the influence of surface compliance on the production of sound by a turbulent boundary layer Howe (1983) has shown that a similar sort of higher-order interaction produces powerful additional noise sources in flows over Kramer-type surfaces.

has been focused on the TSI only, whereas in many cases there are two or more modes of instability present. Lastly, internal damping has hitherto been characterized by a constant damping coefficient. For an actual compliant coating, however, the damping is due both to viscous effects in the substrate fluid and to the viscoelastic properties of the solid part of the coating. It is not clear what value should be assigned to the damping coefficient in order to model the effects of a substrate fluid of given viscosity and/or a solid material of given viscoelastic properties. Moreover, since the damping properties of a viscous fluid substrate and a viscoelastic material actually vary with frequency and wavelength, it is evident that the use of a constant damping coefficient will not model the real damping properties completely satisfactorily.

These points have been borne in mind in developing the theoretical model for the compliant coating presented below and in applying the present theoretical methods.

3. Theoretical model for the compliant surface

3.1. *Description of model*

A fairly general theoretical model for a compliant coating is illustrated schematically in figure 5. It consists of an elastic plate (or tensioned membrane) supported above a rigid surface by an array of springs. The plate is backed by a fluid substrate which, in general, has a different density and viscosity from the main flow. It is assumed that the effect of the springs on the motion of the plate can be modelled by a continuous elastic foundation, of stiffness K. This should be a reasonable approximation provided that the wavelength of the surface instabilities considerably exceeds the distance between neighbouring springs. It is also assumed that the presence of the springs has a negligible effect on the motion of the substrate fluid. This theoretical model should be applicable to many of the compliant surfaces previously studied, including those of Kramer.

If such a surface undergoes two-dimensional disturbances the motion of the surface will be governed by the following equation (see, for example, Kornecki 1978):

$$\rho_{\mathrm{m}} b \frac{\partial^2 w}{\partial t^2} + d \frac{\partial w}{\partial t} + B \frac{\partial^4 w}{\partial x^4} - T \frac{\partial^2 w}{\partial x^2} + \{K - g(\rho_{\mathrm{e}} - \rho_{\mathrm{s}})\} w = \delta p_{\mathrm{s}} - \delta p_{\mathrm{e}}, \tag{3.1}$$

where w is the surface displacement, ρ_{m}, ρ_{e} and ρ_{s} are respectively the densities of the plate material, main flow and substrate fluid, b is the plate thickness, d is a damping coefficient, B is the flexural rigidity of the plate, T is the longitudinal tension per unit width, and K is the spring stiffness per unit width. δp_{e} and δp_{s} are, respectively, the perturbations in dynamic pressure acting on the plate from above and below. The perturbations in hydrostatic pressure are included in the last term on the left-hand side of (3.1) since it is convenient to introduce an equivalent spring stiffness defined as

$$K_{\mathrm{E}} = K - g(\rho_{\mathrm{e}} - \rho_{\mathrm{s}}). \tag{3.2}$$

The flexural rigidity is given by

$$B = \frac{E b^3}{12(1-\nu^2)}, \tag{3.3}$$

where E and ν are respectively the Young's modulus and Poisson's ratio of the plate material.

For a travelling-wave type of disturbance the surface displacement takes the form:

$$w = w_0 \exp\{\mathrm{i}\alpha(x - ct)\}, \tag{3.4}$$

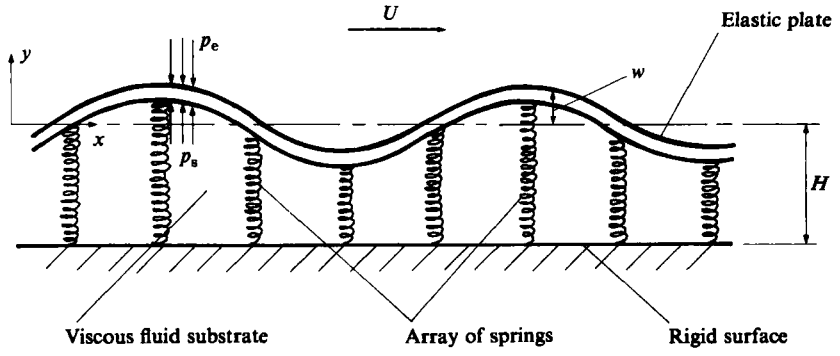

FIGURE 5. A schematic illustration of the theoretical model for a compliant coating.

where α is the wavenumber and c is the complex wave speed. Let the corresponding expressions for the dynamic pressure perturbations be given by

$$\delta p_e = \rho_e U_\infty^2 \hat{p}_e \bar{w} \quad \text{and} \quad \delta p_s = \rho_e U_\infty^2 \hat{p}_s \bar{w}, \tag{3.5}$$

where U_∞ is the free-stream speed and $\bar{w} = w/\delta^*$. If (3.4) and (3.5) are substituted in (3.1) and both sides divided by $\rho_e U_\infty^2 \bar{w}$, (3.1) can be written as

$$-\bar{\alpha}^2\bar{c}^2 C_M - i\bar{\alpha}\bar{c} C_D + \bar{\alpha}^4 C_B + \bar{\alpha}^2 C_T + C_{KE} = \hat{p}_s - \hat{p}_e. \tag{3.6}$$

Here $\bar{\alpha}$ and $\bar{c}$ are non-dimensional wavenumber and complex wavespeed, respectively, defined by

$$\bar{\alpha} = \alpha\delta^* \quad \text{and} \quad \bar{c} = \frac{c}{U_\infty}. \tag{3.7}$$

The non-dimensional coefficients describing the mechanical properties of the coating are defined as follows:

$$\left.\begin{aligned} C_M = \frac{b\rho_m}{\rho_e \delta^*}, \quad C_D = \frac{d}{\rho_e U_\infty}, \quad C_B = \frac{B}{\rho_e U_\infty^2 \delta^{*3}}, \\ C_T = \frac{T}{\rho_e U_\infty^2 \delta^*} \quad \text{and} \quad C_{KE} = \frac{K_E \delta^*}{\rho_e U_\infty^2}. \end{aligned}\right\} \tag{3.8}$$

In order to obtain solutions to the Orr–Sommerfeld equation (see §4) it is necessary to use (3.6) to obtain an expression for the surface admittance. Before this can be done an expression must be derived for the non-dimensional substrate pressure, $\hat{p}_s$.

Elastomeric materials are used for the plates (or membranes) and/or spring foundation of most compliant surfaces. Consequently, it is necessary to take the viscoelastic nature of the materials into account in order to obtain a realistic model. Suppose that the behaviour of the material can be reasonably approximated by the Standard Linear Solid† model, i.e. the stress σ and rate of stress $\dot{\sigma}$ are related to the strain ϵ and rate of strain $\dot{\epsilon}$ as follows:

$$a_0\sigma + a_1\dot{\sigma} = b_0\epsilon + b_1\dot{\epsilon},$$

where a_0, a_1, b_0 and b_1 are constants. Let us consider a rod of this material subjected to a sinusoidally varying direct stress so that $\sigma \sim e^{-i\omega t}$ and $\epsilon \sim e^{-i\omega t}$. Then from the constitutive equation given above it can be seen that

$$(a_0 - i\omega a_1)\sigma = (b_0 - i\omega b_1)\epsilon.$$

† This is the most general of the classical models, but the arguments given above apply equally well to the much more general constitutive equations first studied by Alfrey (1944).

This relationship between stress and strain can be formally regarded as equivalent to the introduction of a complex elastic modulus E^* such that

$$E^* = E(1-\mathrm{i}\eta), \quad \eta = |E_\mathrm{i}^*/E_\mathrm{r}^*|, \tag{3.9}$$

where E_i^* and E_r^* denote respectively the imaginary and real parts of E^*. The symbol E is retained for E_r^* and the loss factor η is introduced. Experimental data are readily available giving the variation of E and η with frequency and temperature for many elastomers.

If it is assumed that both B and K are proportional to E^* then C_B and C_{KE} in (3.6) can be replaced respectively by $C_B(1-\mathrm{i}\eta)$ and $C_{KE}(1-\mathrm{i}\eta')$, the loss factors η and η' being different, in general, in order to take account of the contribution of hydrostatic pressure perturbations and possible differences in material.

3.2. *Derivation of an expression for substrate pressure*

Since the motion of the substrate fluid is due solely to the motion of the plate, which arises from the small disturbance, it can be assumed that the velocities are low. This allows the Navier–Stokes equations to be linearized, giving

$$\rho_\mathrm{s}\frac{\partial u_\mathrm{s}}{\partial t} = -\frac{\partial p_\mathrm{s}}{\partial x} + \mu_\mathrm{s}\left[\frac{\partial^2 u_\mathrm{s}}{\partial x^2} + \frac{\partial^2 u_\mathrm{s}}{\partial y^2}\right], \tag{3.10}$$

$$\rho_\mathrm{s}\frac{\partial v_\mathrm{s}}{\partial t} = -\frac{\partial p_\mathrm{s}}{\partial y} + \mu_\mathrm{s}\left[\frac{\partial^2 v_\mathrm{s}}{\partial x^2} + \frac{\partial^2 v_\mathrm{s}}{\partial y^2}\right], \tag{3.11}$$

where u_s and v_s are the velocity components in the x- and y-directions respectively, and μ_s is the dynamic viscosity of the substrate fluid.

A stream function for the substrate fluid motion is introduced having the form

$$\psi_\mathrm{s} = F_\mathrm{s}(y)\exp\{\mathrm{i}\alpha(x-ct)\}, \tag{3.12}$$

so that

$$u_\mathrm{s} = \frac{\partial \psi_\mathrm{s}}{\partial y} = F_\mathrm{s}'(y)\exp\{\mathrm{i}\alpha(x-ct)\} \tag{3.13}$$

and

$$v_\mathrm{s} = -\frac{\partial \psi_\mathrm{s}}{\partial x} = -\mathrm{i}\alpha F_\mathrm{s}(y)\exp\{\mathrm{i}\alpha(x-ct)\}. \tag{3.14}$$

Equations (3.13) and (3.14) are substituted into (3.10) and (3.11), and p_s is then eliminated by cross differentiation to obtain the following fourth-order ordinary differential equation for F_s:

$$\alpha c(F_\mathrm{s}''-\alpha^2 F_\mathrm{s}) - \mathrm{i}\nu_\mathrm{s}(\alpha^4 F_\mathrm{s} - 2\alpha^2 F_\mathrm{s}'' + F_\mathrm{s}^{\mathrm{iv}}) = 0. \tag{3.15}$$

Equation (3.15) is, in fact, the Orr–Sommerfeld equation with the mainstream velocity set equal to zero. The general solution to (3.15) is given by

$$F_\mathrm{s} = A_1\,\mathrm{e}^{\alpha y} + A_2\,\mathrm{e}^{-\alpha y} + A_3\,\mathrm{e}^{\beta y} + A_4\,\mathrm{e}^{-\beta y}, \tag{3.16}$$

where

$$\beta^2 = \alpha^2 - \frac{\mathrm{i}\alpha c}{\nu_\mathrm{s}}. \tag{3.17}$$

The boundary conditions are

$$\left.\begin{aligned} &u_\mathrm{s} = 0 \quad \text{and} \quad v_\mathrm{s} = \frac{\partial w}{\partial t} \quad \text{at } y = 0, \\ &u_\mathrm{s} = v_\mathrm{s} = 0 \quad \text{at } y = -H. \end{aligned}\right\} \tag{3.18}$$

Here, it is assumed implicitly that any streamwise motion of the compliant surface is negligible, and hence $u_s = 0$ at $y = 0$. From (3.4), (3.13) and (3.14) it can be seen that (3.18) are equivalent to

$$F_s(0) = cw_0, \quad F_s'(0) = F_s(-H) = F_s'(-H) = 0. \tag{3.19}$$

The constants of integration A_1 etc. can be evaluated by applying conditions (3.19) to the expression (3.16).

Substitution of (3.13), (3.14) and (3.5) with (3.4) into equation (3.10) gives, after rearrangement, the following expression for the dynamic pressure perturbation at the compliant surface:

$$\hat{p}_s = \frac{(\rho_s c + i\mu_s \alpha) F_s'(0) - i\mu_s F_s'''(0)/\alpha}{\bar{w}_0 \rho_e U_\infty^2}. \tag{3.20}$$

With the use of boundary conditions (3.19) and equation (3.16) it can be shown that

$$\hat{p}_s = \frac{\bar{\alpha}\rho_s c(A_1 - A_2)}{\bar{w}_0 \rho_e U_\infty^2}. \tag{3.21}$$

A_1 and A_2 may be evaluated by applying the boundary conditions (3.19), as explained above, to give

$$\hat{p}_s = \frac{\bar{\alpha}\rho_s c^2}{\rho_e U_\infty^2}\left(\frac{\bar{\beta}(\bar{\beta}+\bar{\alpha})\{e^{(\bar{\beta}-\bar{\alpha})\bar{H}} - e^{-(\bar{\beta}-\bar{\alpha})\bar{H}}\} + \bar{\beta}(\bar{\beta}-\bar{\alpha})\{e^{(\bar{\beta}+\bar{\alpha})\bar{H}} - e^{-(\bar{\beta}+\bar{\alpha})\bar{H}}\}}{8\bar{\alpha}\bar{\beta} + (\bar{\beta}-\bar{\alpha})^2\{e^{(\bar{\beta}+\bar{\alpha})\bar{H}} + e^{-(\bar{\beta}+\bar{\alpha})\bar{H}}\} - (\bar{\beta}+\bar{\alpha})^2\{e^{(\bar{\beta}-\bar{\alpha})\bar{H}} + e^{-(\bar{\beta}-\bar{\alpha})\bar{H}}\}}\right), \tag{3.22}$$

where $$\bar{\beta} = \beta\delta^* \quad \text{and} \quad \bar{H} = H/\delta^*.$$

This expression can be substituted for $\hat{p}_s$ in (3.6). It can be seen that in general the relationship between $\hat{p}_s$ and c is fairly complex. There are two simpler special cases, however.

If $\nu_s \to 0$ then (3.22) reduces to

$$\hat{p}_s = \frac{\bar{\alpha}\rho_s c^2}{\rho_e U_\infty^2}\left(\frac{1 + e^{-2\bar{\alpha}\bar{H}}}{1 - e^{-2\bar{\alpha}\bar{H}}}\right). \tag{3.23}$$

This is the appropriate form for an inviscid substrate fluid.

If $H \to 0$ for fixed ν_s then (3.22) reduces to

$$\hat{p}_s = \frac{12i\bar{\alpha}^2\mu_s c}{\delta^*\rho_e U_\infty^2(\bar{\alpha}\bar{H})^3}. \tag{3.24}$$

Equation (3.24) is a fair approximation for small substrate depths and high viscosities. It can be seen from its form that under this small depth approximation the effect of a viscous fluid substrate is equivalent to a conventional damping term of the form $d\,\partial w/\partial t$ in (3.1). The equivalent damping coefficient takes the form

$$d = \frac{12\alpha\mu_s}{(\alpha H)^3}. \tag{3.25}$$

With d evaluated according to (3.25), $\hat{p}_s$ can be replaced by a term of the form $i\bar{\alpha}\bar{c}C_D$ in (3.6).

3.3. *Evaluation of parameters for Kramer coatings*

Kramer's tests were carried out in the sea. The temperature of the water was not given, but must have been about 10 °C, to judge from the value of 1.37×10^{-6} m^2/s for the kinematic viscosity which may be deduced from the values he cites for

Reynolds number. The density of sea water is about 1025 kg m^{-3}. The damping fluids used were silicone fluids, the density of which rises slightly with their nominal viscosity. For a nominal viscosity of 300 cSt (the optimum value for Kramer's best coating) the density is about 970 kg m^{-3} according to Meals (1969). The viscosity of such fluids varies very markedly with temperature according to the Walther equation, namely

$$\log\log(\nu+0.8) = A\log T + C. \tag{3.26}$$

In (3.26) ν must be expressed in cSt and the temperature T in degrees Rankine. The constants A and B for a nominal viscosity of 300 cSt at 25 °C may be obtained by interpolation from Meals' figure 3. In this way a value of 450 cSt corresponding to 10 °C was obtained from (3.26). So for Kramer's best coating the following non-dimensional ratios are obtained:

$$\frac{\rho_s}{\rho_e} = 0.946, \quad \frac{\nu_s}{\nu_e} \simeq 335.$$

The above value of ρ_s/ρ_e is used throughout but values of the viscosity ratio vary.

Kramer (1962) states that the softest natural rubbers available for manufacturing his coatings had an elastic modulus of about 0.4 N mm^{-2}. It also appears from the information given in this later paper that the hardest of the three rubbers used for his original coatings had an elastic modulus of about 1.0 N mm^{-2}. The values of the coating stiffnesses were obtained by using an indenter type of instrument which measured the depth of deformation due to an applied point load. With this type of test it would be expected that most of the point load would be supported by a single stub, in which case the elastic modulus would vary linearly with coating stiffness. Assuming that the lowest coating stiffness of 0.167 N mm^{-3} quoted by Kramer corresponds to $E = 0.4$ N mm^{-2}, we obtain the relationship

$$E(\text{in N m}^{-2}) = 2.395\times10^{-3}\times(\text{coating stiffness in N m}^{-3}). \tag{3.27}$$

In this way the values of E given in table 1 are obtained for Kramer's three coatings (see figure 3). The fact that the predicted value of E for the stiffest coating (B) corresponds closely to the highest value available for E suggests that (3.27) is fairly accurate.

As suggested above, the coating stiffness measured by Kramer corresponds, roughly at least, to a nominally point load which is largely supported by a single stub. However, this is not the appropriate way to calculate the stiffness for a relatively long-wave sinusoidal periodic pressure perturbation. In this case it can be assumed that the pressure acting on the surface is supported by a large number of stubs. From the geometric parameters given in figure 1 (*b*) it can be calculated that the total cross-sectional area of the stubs is 1/(4.4) times the total surface area of the coating, so that it can be estimated that the pressure supported by the stubs is 4.4 times the surface pressure. Given that the undeformed height of a stub is 1 mm, it follows that the spring stiffness is given by

$$K = \frac{E}{4.4\times10^{-3}} = 230E \text{ N m}^{-3}. \tag{3.28}\dagger$$

Note that the values of stiffness given in table 1 are almost half those given in (3.28).

For natural rubber the density is about 945 kg m^{-3} and the Poisson's ratio is close to 0.5. From figure 1 (*a*) it can be seen that the plate thickness $b = 2$ mm. Thus from (3.3) we obtain

$$B = 8.9\times10^{-10}\times E \text{ N m}. \tag{3.29}\dagger$$

† The units of E are N m^{-2} in these formulae.

Coating (see figure 3)	Kramer's measured coating stiffness (N mm^{-3})	Elastic modulus (from (3.27)) (N mm^{-2})
B	0.434	1.04
C	0.217	0.52
D	0.167	0.40

TABLE 1. Values of coating stiffness and elastic modulus for Kramer's surfaces

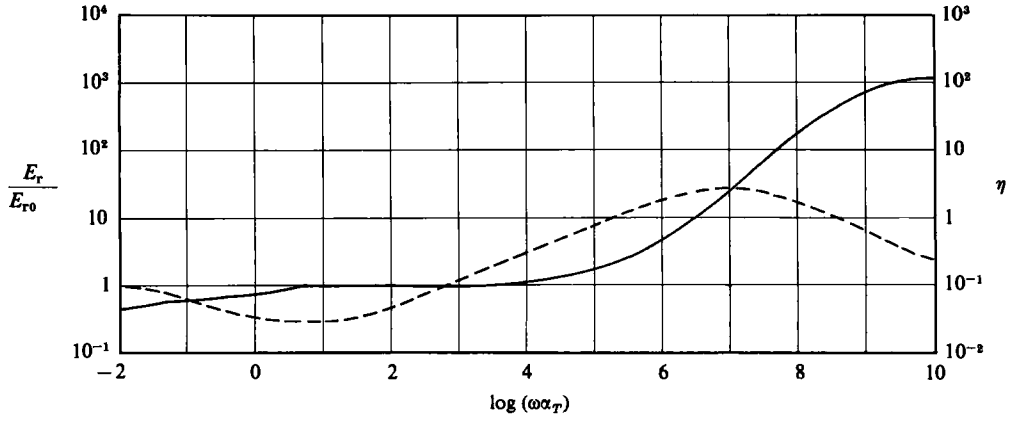

FIGURE 6. The variation of storage elastic modulus and loss factor with a combined frequency–temperature parameter for unvulcanized natural rubber. (Based on figure 3 of Payne 1958): ——, E_r/E_{r0}; ---, η; $\log a_T = -8.86(T-273)/(T-171.4)$.

Kramer makes no mention of any tension being applied to the coatings, so it is assumed that only sufficient tension is applied to keep the coating firmly and smoothly attached to the rigid part of the model. Consequently, for calculations we take $T = 0$.

The maximum speed for Kramer's tests was 18 m/s and this is the value of U_∞ used for most of the calculations. Some calculations are also carried out for 15 m/s.

The plate and the springy stubs in Kramer's coating are both made of the same rubber. Also the contribution of hydrostatic pressure perturbation to K_E in (3.2) is negligible compared to K and so in this case the loss factors η and η' are identical. It is difficult, however, to assign any numerical value to η. A typical variation of storage modulus and loss factor with frequency for natural rubber is shown in figure 6, based on figure 3 of Payne (1958). It can be seen that both quantities vary strongly with frequency. Figure 6 corresponds to a rubber having a nominal storage modulus of $E \approx 3.0$ N mm^{-2} which is considerably stiffer than Kramer's coating B. The curves illustrated in figure 6 vary considerably from one type of rubber to another, so they are not very likely to correspond at all closely to the curves appropriate for the rubbers used by Kramer. Unfortunately, Kramer only characterizes the internal (viscoelastic) damping of his coatings by quoting values for what he termed relative damping. These values were obtained by dropping a 13 mm diameter piston weighing 14 g onto the coating from a height of 51 mm and measuring the height of rebound. The relative damping was defined as the ratio of the rebound height to the original height. Even if it were feasible to deduce a value of loss factor from the value of

relative damping, which it is not, this would still only yield a value for a single frequency at best. Thus we are faced, essentially, with choosing either to use the variations shown in figure 6, which is perfectly feasible with our approach to the problem, or simply to take fixed values of E and η and examine the effect on hydrodynamic stability of changing these values. We chose the latter approach.

4. Formulation of the boundary-layer stability problem

Following the usual procedure, it is assumed that the perturbation is two-dimensional and is described by a stream function which takes the form

$$\psi_e(x, y, t) = \delta^* U_\infty \phi(\bar{y}) \exp\{i\alpha(x-ct)\}, \tag{4.1}$$

where x and y are the streamwise and normal coordinates respectively, t is time, δ^* is the boundary-layer displacement thickness, U_∞ is the free-stream velocity and $\bar{y} = y/\delta^*$. The dimensionless disturbance amplitude ϕ is obtained by solving the Orr–Sommerfeld equation, which takes the form

$$\phi^{iv} - 2\bar{\alpha}^2\phi'' + \bar{\alpha}^4\phi + i\bar{\alpha}\, Re\{(\bar{c}-\bar{U})(\phi''-\bar{\alpha}^2\phi) + \bar{U}''\phi\} = 0, \tag{4.2}$$

where $\bar{\alpha} = \delta^*\alpha$, $Re = U_\infty \delta^*/\nu_e$, $\bar{c} = c/U_\infty$, ν_e is the kinematic viscosity of the boundary-layer fluid and $U_\infty \bar{U}(\bar{y})$ is the mean flow velocity in the boundary layer.

The boundary conditions at the outer edge of the boundary layer are the same for both rigid and flexible surfaces. The two fundamental solutions of (4.2) which decay as $\bar{y} \to \infty$ are given by $\exp(-\bar{\alpha}\bar{y})$ and $\exp(-\bar{\beta}_1 \bar{y})$ for $\bar{y} \gtrsim 3$ where $\bar{\beta}_1^2 = \bar{\alpha}^2 + i\bar{\alpha}\, Re\,(1-\bar{c})$, real part of $\bar{\beta}_1$, $(\bar{\beta}_1)_r > 0$. The appropriate boundary conditions are determined by the form of these fundamental solutions. Because of the numerical methods used for the present work it is convenient to put these boundary conditions in the form

$$\left.\begin{aligned}(D+\bar{\alpha})(D^2-\bar{\beta}_1^2)\phi(3) = 0,\\ (D+\bar{\beta}_1)(D^2-\bar{\alpha})\phi(3) = 0,\end{aligned}\right\} \tag{4.3}$$

where D denotes $d/d\bar{y}$. The application of these boundary conditions at $\bar{y} = 3$ follows from the fact that at a distance of just under $3\delta^*$ from the surface of a flat plate $\bar{U} = 0.99$ (for example, see Schlichting 1968) and therefore, to a good approximation, potential flow can be assumed for $\bar{y} > 3$.

In the case of the rigid wall the boundary conditions at the wall are given by the requirements of zero normal velocity and no slip. This gives

$$\phi(0) = 0, \quad \phi'(0) = 0. \tag{4.4a,b}$$

For a flexible surface, particularly the types studied in the present paper, it is still reasonable to assume that the no-slip condition holds. Let the non-dimensional surface deformation be given by

$$\bar{w} = \frac{w}{\delta^*} = \bar{w}_0 \exp\{i\alpha(x-ct)\}. \tag{4.5}$$

Similarly, let the streamwise and normal velocity components and pressure be given by

$$u_e = U_\infty \bar{u}_e = U_\infty \hat{u}_e(\bar{y}) \exp\{i\alpha(x-ct)\}, \tag{4.6a}$$

$$v_e = U_\infty \bar{v}_e = U_\infty \hat{v}_e(\bar{y}) \exp\{i\alpha(x-ct)\}, \tag{4.6b}$$

$$p_e = \rho_e U_\infty^2 \bar{p}_e = \rho_e U_\infty^2 \hat{p}_e(\bar{y})\, \bar{w}_0 \exp\{i\alpha(x-ct)\}, \tag{4.6c}$$

where ρ_e is the density of the boundary-layer fluid.

It is easy to show (e.g. see Benjamin 1960 or Landahl 1962) that the no-slip condition implies that

$$\phi(0)\,\bar{U}'(0)+\bar{c}\phi'(0)=0. \tag{4.7}$$

Following Landahl (1962) and Landahl & Kaplan (1965) the concept of admittance is introduced, where

$$Y=-\frac{\text{normal velocity}}{\text{applied pressure}}. \tag{4.8}$$

At the flexible surface the pressure and normal velocity of the boundary-layer fluid must be the same as those in the flexible medium. So at the surface $\bar{y}=0$,

$$Y_0=Y_1 \tag{4.9}$$

where Y_0 and Y_1 are, respectively, the admittances of the boundary-layer fluid and flexible surface. When suitable expressions are derived for Y_0 and Y_1, (4.9) acts as the fourth boundary condition at the flexible wall, replacing the condition (4.4*a*) used for the rigid wall.

Landahl (1962) showed that a suitable expression for Y_0 can be derived from the linearized x-momentum equation. In the case when the no-slip condition (4.7) holds, his expression takes the form

$$Y_0=-\frac{\bar{v}_e(0)}{\bar{p}_e(0)}=\frac{-\bar{\alpha}^2\,Re\,\phi(0)}{\phi'''(0)-\bar{\alpha}^2\phi'(0)}. \tag{4.10}$$

The admittance for the flexible surface is given by

$$Y_1=-\frac{\partial\bar{w}/\partial t}{\delta p_e/(\rho_e U_\infty^2)}, \tag{4.11}$$

which, with use of (3.4), (3.5) and (3.6), can be written as

$$Y_1=\frac{i\bar{\alpha}\bar{c}}{\hat{p}_s+\bar{\alpha}^2\bar{c}^2C_M+i\bar{\alpha}\bar{c}C_D-\bar{\alpha}^4C_B-\bar{\alpha}^2C_T-C_{KE}}. \tag{4.12}$$

$\hat{p}_s$ is evaluated by using (3.22) and, when the viscoelastic properties of the plate and springs are taken into account, C_B and C_{KE} are multiplied by $(1-\eta)$ and $(1-\eta')$ respectively.

5. Approximate theory

The approximate theory presented in this section is based in part on the method devised by Landahl (1962) for determining the optimum surface properties of compliant surfaces. Its main purpose here is to determine whether making a particular change to the mechanical properties of the flexible surface is likely to be stabilizing or destabilizing.

The free-wave speed of the type of flexible surface under consideration is given, in the most general form, by

$$c_0=\left\{\frac{\alpha^2B+T+K_E/\alpha^2}{b\rho_m}\right\}^{\frac{1}{2}}. \tag{5.1}$$

So the non-dimensional free-wave speed can be defined as

$$\bar{c}_0=\left\{\frac{\bar{\alpha}^2C_B+C_T+C_{KE}\bar{\alpha}^{-2}}{C_M}\right\}^{\frac{1}{2}}. \tag{5.2}$$

With use of (5.2) in (4.12), the boundary condition (4.9) may be written as

$$Y_0+\frac{\mathrm{i}\bar{c}}{\bar{\alpha}C_M(\bar{c}_0^2-\bar{c}^2)-\mathrm{i}\bar{c}C_D-\hat{p}_s/\bar{\alpha}}=0. \tag{5.3}$$

Let the unperturbed state correspond to a flexible surface with no fluid substrate and no damping, so that $C_D=\hat{p}_s=0$. Also let the unperturbed state be neutrally stable with $\bar{c}=a$ (a is real). In the most general case it is assumed that a slight departure from this unperturbed state comes about because of small changes to the mechanical properties of the surface (so that small changes occur to C_M and $\bar{c}_0^2$), and by introducing a fluid substrate and damping (so that C_D and $\hat{p}_s$ are small quantities). These small changes will bring about a small change in complex-wave speed, so that in the perturbed state

$$\bar{c}=a+\Delta\bar{c}, \tag{5.4}$$

where $|\Delta\bar{c}|\ll a$.

For the perturbed state, (5.3) can be written as

$$Y_0+\left(\frac{\partial Y_0}{\partial\bar{c}}\right)_{\bar{c}=a}\Delta\bar{c}+\frac{\mathrm{i}(a+\Delta\bar{c})}{\bar{\alpha}C_M(\bar{c}_0^2-a^2)-2\bar{\alpha}C_M a\,\Delta\bar{c}+\epsilon}=0, \tag{5.5}$$

where

$$\epsilon=\bar{\alpha}\Delta(C_M\bar{c}_0^2)-\bar{\alpha}a^2\Delta C_M-\mathrm{i}aC_D-\frac{\hat{p}_s}{\bar{\alpha}} \tag{5.6}$$

and $\Delta(C_M\bar{c}_0^2)$ and ΔC_M denote the small changes in $C_M\bar{c}_0^2$ and C_M respectively. ϵ is an overall small parameter encompassing all of the various small changes possible in the properties of the flexible surface. Using (5.3), applying the binomial theorem to the denominator of the last term on the right-hand side of (5.5) and neglecting higher-order terms, (5.5) can be rearranged to give

$$\Delta\bar{c}\left[\left(\frac{\partial Y_0}{\partial\bar{c}}\right)_{\bar{c}=a}+\frac{\mathrm{i}\bar{\alpha}C_M(\bar{c}_0^2+a^2)}{\{\bar{\alpha}C_M(\bar{c}_0^2-a^2)\}^2}\right]=\frac{\mathrm{i}a\epsilon}{\{\bar{\alpha}C_M(\bar{c}_0^2-a^2\}^2}. \tag{5.7}$$

The main purpose of this approximate theory is to determine whether a certain small change to the properties of the flexible surface is destabilizing or stabilizing. This information can be obtained by using (5.7) to determine the sign of $\Delta\bar{c}_\mathrm{i}$ (the imaginary part of $\Delta\bar{c}$). From (5.7) we find that the sign of $\Delta\bar{c}_\mathrm{i}$ is given by

$$\Delta\bar{c}_\mathrm{i}\sim\frac{a}{\{\bar{\alpha}C_M(\bar{c}_0^2-a^2)\}^2}\left(\epsilon_\mathrm{R}R_Y+\epsilon_\mathrm{I}I_Y+\frac{\epsilon_\mathrm{I}\bar{\alpha}C_M(\bar{c}_0^2+a^2)}{\{\bar{\alpha}C_M(\bar{c}_0^2-a^2)\}^2}\right), \tag{5.8}$$

where ϵ_R and ϵ_I are the real and imaginary parts, respectively, of ϵ and R_Y and I_Y are the real and imaginary parts, respectively, of $(\partial Y_0/\partial\bar{c})_{\bar{c}=a}$. The sign of R_Y and I_Y can be deduced approximately from figure 5 of Landahl (1962), which shows that $R_Y\gtrsim 0$ and $I_Y<0$ for the range of $\bar{c}$ involved in TSI on rigid surfaces.

A number of special cases will be considered below.

Effects of changing free wave speed or plate mass

Suppose that the flexural rigidity, tension or spring stiffness is reduced keeping the mass of the plate (or membrane) fixed. In this case $\Delta(C_M\bar{c}_0)<0$ and $\Delta C_M=0$. So, provided there is no damping and no fluid substrate, it follows from (5.6) that $\epsilon_\mathrm{R}<0$ and $\epsilon_\mathrm{I}=0$. In this case (5.8) implies that $\Delta\bar{c}_\mathrm{i}<0$ (i.e. stability) provided $\bar{c}_0>a$ and $R_Y>0$. Both of these conditions are satisfied for TSI on Kramer-type flexible surfaces (and probably on most other compliant surfaces also). Thus it can be

concluded that a reduction in flexural rigidity, tension and/or spring stiffness, keeping plate mass fixed, has a stabilizing effect on TSI. Conversely an increase in any of these quantities is destabilizing.

On the other hand, a similar analysis to the one given above shows that a reduction in C_M, keeping $\bar{c}_0^2 C_M$ fixed, has a destabilizing effect on TSI. At first sight this conclusion would seem to contradict the oft-repeated statements of Landahl & Kaplan (1965), Gyorgyfalvy (1967) and others that a low relative mass is one of the principal requirements for a compliant surface capable of delaying transition. In fact, the present conclusion is in agreement with the results illustrated in figure 7 of Landahl (1962). This figure shows that the optimum value of C_M (which corresponds to Landahl's mass parameter denoted by m) is infinite for the case of zero damping. The introduction of fairly light damping, though, drastically reduces the optimum value of C_M according to Landahl's results. It is worth pointing out, however, that a substrate fluid of low viscosity (e.g. water) can be used for Kramer surfaces. In this case our results (see §7.3) indicate that the surface behaves almost the same as one with an inviscid fluid substrate. In practice, of course, it is not possible to raise the mass of the plate indefinitely without increasing the flexural rigidity, which has a destabilizing effect. Presumably it is the trade-off between these two effects which determines the optimum value of C_M in practice.

Effect of an inviscid fluid substrate

Suppose that the mechanical properties of the plate (or membrane) and spring foundation remain unchanged, but an inviscid fluid substrate is introduced. In this case, using (3.23) with (5.6),

$$\epsilon = -\frac{a^2(\rho_s/\rho_e)\,(1+e^{-2\alpha H})}{1-e^{-2\alpha H}} \tag{5.9}$$

so that $\epsilon_R < 0$ and $\epsilon_I = 0$. As before this implies that $\Delta c_i < 0$ so an inviscid substrate fluid has a stabilizing effect on TSI.

Effect of a viscous fluid substrate

In general, for a viscous fluid substrate, (3.22) should be used for $\hat{p}_s$. It would, however, be a tedious, and ultimately unrewarding, task to split (3.22) into its real and imaginary parts. Consequently, the simple approximate result (3.24) will be used instead. In this case

$$\epsilon = -\frac{12i\bar{\alpha}(\mu_s/\mu_e)\,\bar{c}}{\{Re\,(\alpha H)^3\}}, \tag{5.10}$$

so that $\epsilon_R = 0$ and $\epsilon_I < 0$. This is exactly analogous to the effects of conventional damping (i.e. $C_D \neq 0$) which Benjamin (1960), Landahl (1962) and others have found has a destabilizing effect on the TSI. Using the present procedure, it can be seen that, of the three terms in the large brackets on the right-hand side of (5.8), the first is equivalently zero, the second is positive and the third is negative. Therefore, the sign of $\Delta\bar{c}_i$ depends on the relative magnitude of the last two terms. If $\bar{c}_0 \gg a$ (a good approximation for TSI) the last term reduces to $\epsilon_I/\{\bar{\alpha}(C_M\,\bar{c}_0^2\}$. It can be seen from figure 5 of Landahl (1962) that I_Y lies between about -0.7 and -1.0 while for Kramer's best coating $\bar{\alpha}C_M\,\bar{c}_0^2$ is about 5.0.† So, in this case at least, $|I_Y|$ exceeds $\{\bar{\alpha}C_M\,\bar{c}_0^2\}^{-1}$ by a substantial margin and $\Delta\bar{c}_i > 0$. This seems to be generally true for

† δ was used as reference length in these estimates instead of δ^*.

the TSI, so it follows, in agreement with previous results, that conventional damping and viscous substrates destabilize the TSI.

For very flexible surfaces $\bar{\alpha}C_M\,\bar{c}_0^2$ will be very small, implying $\Delta\bar{c}_i < 0$, but in these cases the surface will be highly unstable to the FISI. Damping will also have a stabilizing effect when $|\bar{c}_0^2 - a^2| \ll 1$. This condition is typical of the travelling-wave flutter FISI for which damping is, indeed, stabilizing (see results in §7.4).

Effect of viscoelastic damping

To allow for viscoelastic effects a complex elastic modulus is introduced (see §3.1). In effect, this means that C_B and C_{KE} are replaced by $C_B(1-\mathrm{i}\eta)$ and $C_{KE}(1-\mathrm{i}\eta')$ respectively. If it is assumed that the real parts of these complex terms remain unchanged then

$$\Delta(C_M\,\bar{c}_0^2) = -\mathrm{i}\left(\bar{\alpha}^2 C_B\,\eta + \frac{C_{KE}\,\eta'}{\bar{\alpha}^2}\right). \tag{5.11}$$

So, viscoelastic damping has an analogous effect to viscous and conventional damping.

Travelling-wave flutter FISI

It must be emphasized that the above conclusions, with regard to the effects of various changes on the instability, apply only to TSI. An approximate theory for the travelling-wave flutter FISI will be presented in Part 2; generally, it will be found that any effect which stabilizes the TSI will destabilize the travelling-wave flutter mode.

6. Numerical methods

6.1. *Numerical integration of the Orr–Sommerfeld equation*

The Orr–Sommerfeld equation (3.2) is a fourth-order linear ordinary differential equation with variable complex coefficients. The fact that the coefficients are complex is of little consequence. It simply means that for the purposes of numerical integration the equation is recast as eight, rather than four, first-order differential equations. The main numerical difficulties in integrating the Orr–Sommerfeld equation come about because it is highly stiffly unstable. Owing to the stiffness one fundamental solution changes very rapidly relative to another, as is well known from the asymptotic analytical solutions (see Lin 1945, for example). This highly stiff, and also unstable, characteristic makes the use of conventional numerical schemes impossible.

Two interesting and informative papers have been written by Gersting & Jankowski (1972) and Gersting (1980) on numerical methods for the Orr–Sommerfeld equation. After assessing the information given in these papers we decided to try two numerical schemes specially developed for stiff equations. The two methods are due to Gear (1971) and Scott & Watts (1975). We had little success using a standard variant of Gear's method but found Scott & Watts' scheme, SUPORT, satisfactory provided modal interactions did not occur. SUPORT was used to obtain all the results presented below.

The basis of SUPORT is a variable-step Runge–Kutta–Fehlberg integration scheme designed for the solution of two-point boundary-value problems. It uses superposition coupled with an ortho-normalization scheme. Each time the superposition solutions start to lose their numerical independence, which is a common occurrence when integrating stiff equations, the solution vectors are ortho-normalized

again before the integration proceeds further. The desired solution is then obtained by piecing together the intermediate solutions.

For the purposes of numerical integration the Orr–Sommerfeld equation (4.2) plus its boundary conditions must be formulated as a two-point boundary-value problem. This is accomplished by introducing a normalization condition at $\bar{y} = 0$. This condition takes the form

$$\phi'''(0) - \bar{\alpha}^2\phi'(0) = 1. \tag{6.1}$$

The form of (6.1) stems from the form of an intermediate variable, $\xi = \phi'' - \bar{\alpha}^2\phi$. ξ is introduced to simplify the numerical formulation and it is convenient to place the normalization condition on ξ rather than ϕ.

For the rigid wall (4.3), (4.4*a*) and (6.1) constitute the four boundary conditions. The fifth condition (4.4*b*) serves as a characteristic equation for determining the complex eigenvalue $\bar{c}$ corresponding to given values of Re and $\bar{\alpha}$. In the case of a flexible wall, the boundary conditions are (4.3), (4.7) and (6.1), while (4.9), supplemented by (4.10) and (4.12), acts as the characteristic equation.

The Blasius velocity profile and its second derivative are required as functions of $\bar{y}$ in the Orr–Sommerfeld equation, (4.2). Previous investigators who have sought similar numerical solutions, e.g. Landahl & Kaplan (1965) and Jordinson (1970), have obtained U and U'' from numerical solutions to the Blasius equation. This is a relatively costly procedure in terms of computing time, so we chose the faster, but probably less accurate, course of fitting polynomials to the tabular data presented in Rosenhead (1963) for U and U''. These polynomials were found to fit the data very accurately.

6.2. *Eigenvalue search schemes*

The characteristic equation is of the form

$$E(\bar{\alpha}, \bar{c}, Re) = 0, \tag{6.2}$$

where the function E is either given by $\phi'(0)$ in the rigid-wall case or by $Y_0 - Y_1$ in the flexible-wall case. Re and $\bar{\alpha}$ are given, and $\bar{c}$ is treated as a single complex eigenvalue.

For the earlier computations, presented by Garrad (1980), the eigenvalue search scheme was based on the following Lagrangian interpolation formula:†

$$\bar{c}_{k+1} = \sum_{l=1}^{k} \bar{c}_l \prod_{\substack{j=1 \\ j \neq l}}^{k} \left(\frac{-E_j}{E_l - E_j} \right), \tag{6.3}$$

where $E_j = E(\bar{\alpha}, \bar{c}_j, Re)$. This allows the next estimate of $\bar{c}$ to be found from the k former estimates. No difficulty was encountered in the application of this method to the problems considered by Garrad (1980). Usually three iterations were sufficient to solve (6.2) to within acceptable tolerance. The solutions to these particular problems were not usually too far removed from the ones for a rigid wall. When we attempted to use the method for Kramer-type surfaces, however, serious problems were often encountered. It was frequently found that, unless the initial guess was close to the required solution, the use of (6.3) would not yield a convergent solution. Consequently, the method based on the Lagrangian interpolation formula was abandoned in favour of another.

For the later computations, i.e. the ones presented in the present paper, the method

† This was one of the methods used by Kaplan (1964).

of false position (*regula falsi*) is used (see, e.g., Ostrowski 1960). With this method, which was also used by Kaplan, the $(k+1)$th estimate for $\bar{c}$ is given by

$$\bar{c}_{k+1} = \frac{\bar{c}_{k-1} E_k - \bar{c}_k E_{k-1}}{E_k - E_{k-1}}. \tag{6.4}$$

On the whole this method proved to be superior to the Lagrangian interpolation formula (6.3). No trouble was experienced in finding solutions for non-dissipative walls. However, in certain cases of flexible walls with internal damping serious difficulties were encountered. Very abrupt changes in the character of the eigen-solutions would sometimes occur when the wavenumber or Reynolds number was slightly changed. It is thought that this kind of problem is indicative of some sort of interaction or coalescence between the TSI and FISI. A full investigation of these effects is beyond the scope of the relatively simple methods described above. More suitable methods for investigating modal interactions have been developed by Dr M. Gaster and Mr G. J. K. Willis of NMI Ltd, Teddington (formerly the National Maritime Institute). Some preliminary results are presented by Carpenter, Gaster & Willis (1983) and a more detailed account will be given in Part 3.

6.3. *Redefining the non-dimensional parameters*

Many of the non-dimensional parameters in (3.8), which describe the properties of the flexible surface, depend on the boundary-layer displacement thickness δ^*. In most practical cases the mass, flexural rigidity, tension and spring stiffness do not vary along the surface. On the other hand δ^* increases with distance downstream. Consequently, it is necessary to redefine these parameters each time the value of δ^* (i.e. Re) is changed. This is carried out by designating a more or less arbitrary reference value Re_0 for the Reynolds number. The values of the non-dimensional parameters corresponding to Re_0 are supplied as data and values of the parameters at other values of Re are given by

$$\left.\begin{aligned} C_M &= C_{M0}\frac{Re_0}{Re}, \quad C_D = C_{D0}, \quad C_B = C_{B0}\left(\frac{Re_0}{Re}\right)^3, \\ C_T &= C_{T0}\frac{Re_0}{Re}, \quad C_{KE} = C_{KE0}\frac{Re}{Re_0}, \quad \overline{H} = \overline{H}_0\frac{Re_0}{Re}. \end{aligned}\right\} \tag{6.5}$$

7. Results of numerical analysis

7.1. *Rigid flat plate*

In order to check our numerical methods, a thorough investigation was made of the stability of Blasius flow over a rigid flat plate. The results obtained were compared with previously obtained theoretical and experimental data.

The calculated curve of neutral stability and other curves of constant $\bar{c}_i$ are presented in figure 7. Data points corresponding to the numerical solutions of Kaplan (1964) and Jordinson (1970) are also plotted on figure 7. It can be seen that there is fairly good agreement between the present results and those obtained by the earlier investigators. The critical Reynolds number obtained using the present results is 504 as compared with 518 and 520 obtained by Kaplan and Jordinson respectively. The most unstable wavenumber is found to be $\bar{\alpha} = 0.307$ whereas Kaplan and Jordinson obtained 0.315 and 0.301 respectively. The small discrepancies between the present results and the others are probably caused mainly by differences in the form of

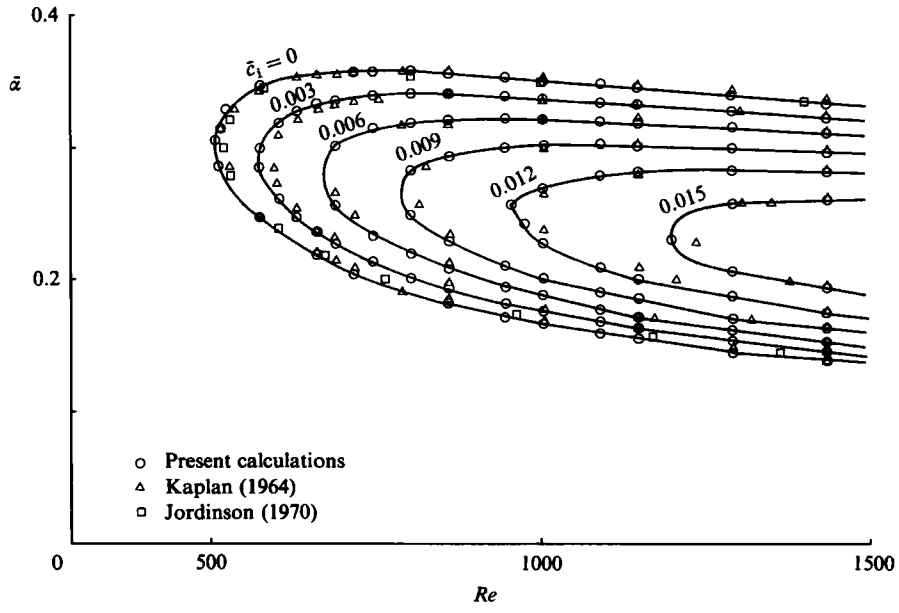

FIGURE 7. Curves of constant $\bar{c}_i$ for Blasius boundary layer on a rigid surface.

mean-velocity profile. Kaplan and Jordinson integrated the Blasius equation numerically to obtain the mean velocity whereas we adopted the less accurate procedure of fitting polynomials to tabular data of U and U''. Other possible reasons for discrepancies are different choices of the value of $\bar{y}$ at which to impose the outer boundary conditions and, in the case of Kaplan, the difficulty of accurately determining his results from his figure 8.

For completeness, comparisons were also made of the amplification rates. In figure 3.6 of Garrad (1980) amplification rates computed by means of the present methods are shown to compare very well with Kaplan's results and the experimental data of Schubauer & Skramstad (1948).

7.2. *Comparison with Landahl & Kaplan's results for spring-backed membrane*

One of the special cases considered by Kaplan (1964) was a compliant surface consisting of a tensioned membrane backed by a spring foundation. There was no substrate fluid but various values of damping coefficient were considered. The neutral curves for such a surface are shown in figures 19 and 21 of Kaplan for various values of damping coefficient. Kaplan's expression for the wall admittance Y_1 was incorporated into our computer program and results obtained for the case shown in Kaplan's figure 21*a*. A comparison between these results and those of Kaplan is presented in figure 3.10 of Garrad (1980). On the whole his results agree reasonably well with those of Kaplan. Garrad's value for critical Reynolds number is 580 as compared with Kaplan's value of 632.

It was realized later by Landahl & Kaplan (1965) that Kaplan's original formula for Y_1 was incorrect. Consequently, a corrected version of the formula was given and revised forms of the calculated neutral curves were presented in figures 6 and 8 of Landahl & Kaplan. We also attempted to compute neutral curves for the case shown in Landahl & Kaplan's figure 8. However, we were unable to find any neutral curves in the range $300 \leqslant Re \leqslant 3100$ and $0.03 \leqslant \bar{\alpha} \leqslant 0.60$.

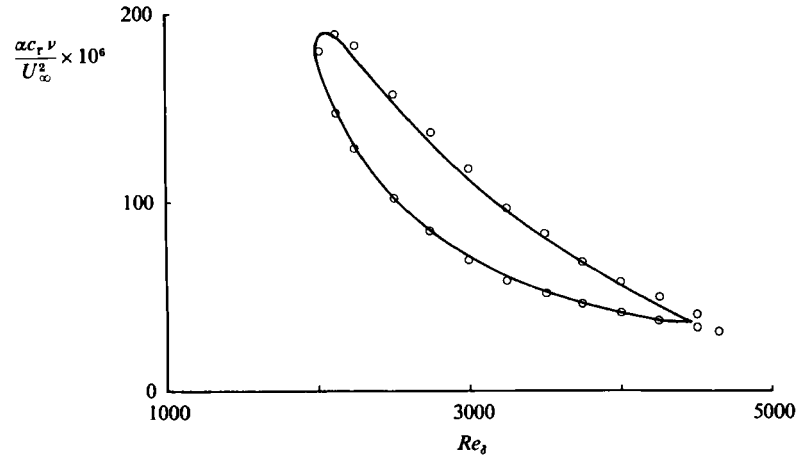

FIGURE 8. Comparison of Landahl & Kaplan's results with those obtained by present methods using (7.1). Spring-backed membrane: $c_0 = 0.5$; $m = 1.0$; $\omega_0 = 0.4$; $R_0 = 5000$; $d = 0.05$; ○, Landahl and Kaplan's results; ——, present results.

Landahl & Kaplan characterized the spring stiffness of the surface by the cut-off frequency $\omega = (K/\rho_m b)^{\frac{1}{2}}$. It was noticed that they stated that the cut-off frequency was made dimensionless by dividing ω by δ/U_∞ (where δ is boundary-layer thickness). This would imply that the relationship between $\bar{\omega}$ and its reference value $\bar{\omega}_0$ is given by

$$\bar{\omega} = \bar{\omega}_0 \frac{Re_0}{Re}. \tag{7.1}$$

In fact, in order to make ω dimensionless one should *multiply* by δ/U_∞, which implies

$$\bar{\omega} = \bar{\omega}_0 \frac{Re}{Re_0}. \tag{7.2}$$

When the incorrect relationship (7.1) was used in our computations the neutral curve shown in figure 8 was obtained† and it can be seen that this curve agrees closely with the results of Landahl & Kaplan. Accordingly we conclude that the results presented in figures 6 and 8 of Landahl & Kaplan are probably incorrect.

7.3. *Comparison between experimental and theoretical results*

Babenko and his colleagues have carried out a series of careful experiments on the hydrodynamic stability of flows over a variety of flexible surfaces: see Babenko (1973*a*) and Babenko & Kozlov (1973). Their results are apparently the only experimental data on stability available for comparison with theory. Babenko (1973*b*) described the methods used to determine the mechanical properties of the flexible surfaces. A detailed description of the test facility and instrumentation was given by Babenko, Gintetskii & Kozlov (1973).

A special low-turbulence water tunnel was designed for the experiments. The water speed could be varied up to 0.15 m/s and the ambient turbulence intensity was 0.04 % during the experiments. The 3 m long working section was fitted with a false floor

† For the results shown in figure 8 the boundary-layer thickness δ is used as a reference length rather than δ^*.

which for the stability experiments either served as the rigid wall or was replaced by various flexible surfaces. A facility was provided for suction at the fore and aft edges of the working section. This helped to maintain a uniform velocity distribution throughout. A camera and related control equipment could be mounted on a carriage which ran on rubber wheels along the top of the working section.

Flow visualization was achieved by means of the tellurium technique, see Wortmann (1953, 1969). This method uses a specially manufactured wire of 0.05 mm diameter coated with tellurium. A continuous or pulsed electric current could be passed through the wire. The instantaneous velocity measurements were made by photographing the colloidal bubble streams emitted from the tellurium wire as it passed a pulsed current. A fairly complex control system was used so that current pulses and triggering of the camera were well synchronized. The wire support was streamlined by means of a plastic cover.

A bronze ribbon, $150 \times 3 \times 0.15$ mm, was positioned upstream of the test section. This could be vibrated mechanically at specific frequencies and amplitudes. The flow disturbance initiated by the vibrating ribbon could be observed by means of the tellurium technique. In order to avoid the occurrence of transition at the ribbon it was necessary to limit the ribbon amplitude to 0.5 mm. In fact an amplitude of 0.32 mm was used for the experiments. For similar reasons the velocity of the ribbon was limited to 2% of the free-stream value.

The curve of neutral stability (in the form of non-dimensional frequency $\bar{\alpha}\bar{c}_r/Re$ vs Re), obtained from the experimental data of Babenko & Kozlov (1973) for a rigid wall, is compared with the experimental data of Schubauer & Skramstadt (1948) in figure 9.† It can be seen that there is reasonable agreement. The experimental data of Ross *et al.* (1970), also shown in figure 9, also agree well with those of Babenko and Kozlov. It can therefore be concluded that the methods used by Babenko *et al.* are basically sound.

Babenko (1973*a*) reported a fairly detailed investigation of flexible surfaces consisting of tensioned polyvinyl-chloride (PVC) membranes stretched over water-filled cavities. The effects on hydrodynamic stability of varying the substrate depth H, the free-stream velocity and the tension were all investigated. It was found that a reduction in substrate depth improved stability. The non-dimensional wavenumber and amplification rate varied little with H but the region of instability was considerably reduced. The normal fluctuating velocity v' was found to be a good indicator of the effect of the surface on the flow. For small values of H small values of v' were recorded. A reduction in the free-stream velocity produced growth in the region of instability and an increase in the wavenumber, phase speed and amplitude of disturbance. Changing the membrane tension had the most marked effect on stability. The surface with the lowest tension produced the best results, the critical Reynolds number being larger than the rigid-wall value by a factor of two.

Owing to the detailed information given by Babenko (1973*a*, *b*) on the simple membrane surfaces and on the results of the experiments it is possible for us to carry out computations on the stability of such surfaces. Two cases (designated B1-B5 and B36-B42 by Babenko) were chosen for theoretical investigation; their specifications are given in table 2. Computed points on the neutral curve are plotted in figure 10. They are almost indistinguishable from the theoretical neutral curve for the rigid wall. Thus it would appear that there is little or no agreement between Babenko's experimental data and the results of the present theory.

† Various theoretical results are also plotted in figure 9 and will be discussed below.

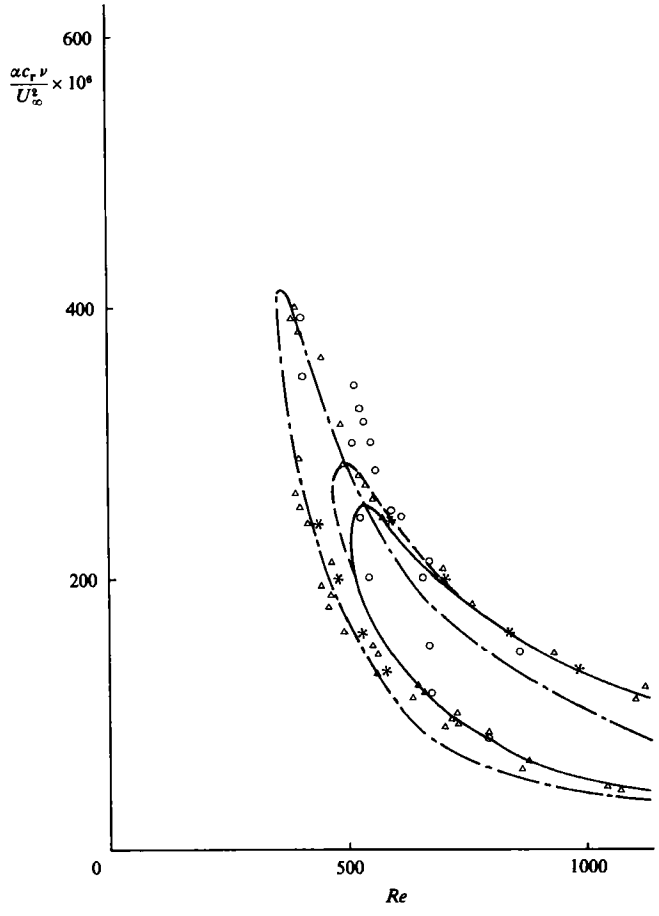

FIGURE 9. Comparison of theoretical neutral curves with experimental data for rigid wall: ——, present results; - - - - -, numerical investigation with boundary layer growth taken into account (Gaster 1974); *, numerical investigation using full Navier–Stokes equations (Fasel 1980); ○, experimental data of Schubauer & Skramstadt (1948); △, experimental data of Ross *et al.* (1970); —·—, experimental curve of Babenko & Kozlov (1973).

Babenko's designation	U_∞ (m/s)	H (mm)	T (N/m)	$\bar{H}_0$	C_{M0}	C_{T0}	Re_0
B1-B5	0.11	70	79	7.666	0.0104	715	1005
B36-B42	0.13	10	25	1.289	0.0123	191	1005

TABLE 2. Parameters for Babenko's flexible surfaces

Before considering the possible reasons for this lack of agreement it is worth pointing out that for the Reynolds-number range investigated by Babenko *et al.* the agreement between theory and experiment is also very poor in the rigid case. For larger Reynolds numbers, however, other investigators have found good agreement between the predictions of linear stability theory and experimental data for the rigid wall. For the lower Reynolds numbers near the critical value the experimental

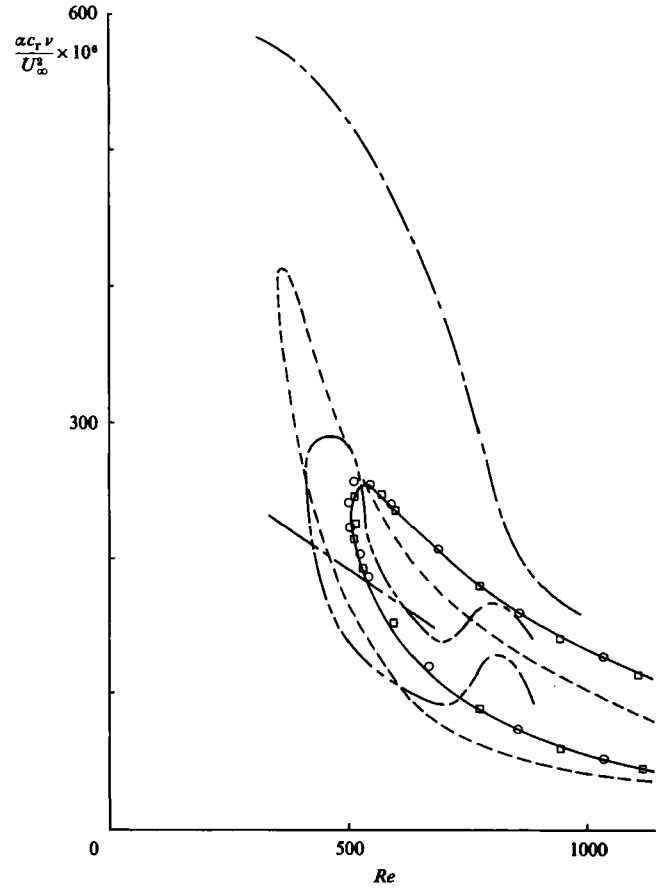

FIGURE 10. Comparison of theoretical neutral curves with experimental data for simple membrane compliant surfaces. Theoretical results using present methods: ——, rigid wall; □, B1-B5 and, ○, B36-B42 of Babenko (1973*a*). Experimental data: - - - - -, rigid wall, Babenko & Kozlov (1973); —·—, B1-B5; and —·-·—, B36-B42 of Babenko (1973*a*).

difficulties are at their most severe. Nevertheless, since the experimental data of Schubauer & Skramstadt, Ross *et al.* and Babenko & Kozlov are more or less in agreement, it is difficult to ascribe the discrepancy between the experimental and theoretical results to experimental error. Accordingly, the discrepancy is probably due to deficiencies in the theory in the case of the rigid wall, at least. It should be remembered that the Orr–Sommerfeld equation is approximate even within the framework of a linear theory. Terms connected with boundary-layer growth are omitted in order to preserve the parallel-flow assumption. When account is taken of the boundary-layer growth, see Gaster (1974) and Barry & Ross (1970), the agreement between the theoretical neutral curve and experimental data is improved, as can be seen in figure 9. There still remains a substantial discrepancy, however. This could very well arise because of the neglected nonlinear terms. Points, corresponding to neutral stability, obtained by Fasel (1980), by means of numerical integration of the full two-dimensional Navier–Stokes equations, are in significantly closer agreement with the experimental data, as can be seen in figure 9. It is difficult, though, to draw firm conclusions from the few points computed by Fasel.

It is readily apparent from figure 10 that, while the theoretical neutral curves are almost identical for the rigid and flexible surfaces, the experimental data for the three surfaces show large differences. The data for the rigid wall and one of the flexible surfaces (B36-B42) are not greatly different but the data for the other flexible wall (B1-B5) are markedly different. Three possible reasons for this difference can be advanced, namely: (i) a different criterion was used to determine instability for the flexible surfaces; (ii) nonlinear effects; (iii) the effects of flow-induced surface instabilities. Each of these will now be considered in turn.

When the small disturbances are represented mathematically in the form (4.1) used for conventional linear theory it does not matter particularly whether one monitors a particular velocity component or an integral quantity, such as the total kinetic energy of the disturbance; the predicted point of instability will not change. However, Gaster (1974) shows that if a more realistic form is chosen to describe the disturbance then it is possible to obtain considerably different results for the point of instability, depending on the quantity chosen to determine instability. In particular, one may expect that a neutral curve obtained by monitoring u' could differ considerably from one obtained by monitoring v'. Babenko & Kozlov do not explain precisely how they determined the point of instability, but it appears that u' may have been used in the rigid case and v' for the flexible surfaces.

Nonlinear effects may be involved in at least two distinct ways. First, there are the direct nonlinear effects on the TSI which are possibly responsible for the discrepancy between theory and experiment in the rigid case. It is only to be expected that these effects will be modified by surface flexibility. With a flexible surface, however, other modes of instability, i.e. FISI, may be present. The possibility also arises, therefore, of a nonlinear interaction between the TSI and the FISI. This interaction may give rise to a much stronger instability. A somewhat similar effect has recently been demonstrated by Howe (1983) in a theoretical study of the influence of surface compliance on the production of sound by a turbulent boundary layer. In this case the flow-induced surface waves induced by a particular component of the boundary-layer pressure fluctuations can interact nonlinearly with another component. Although this is a higher-order effect and had, therefore, been neglected by previous authors, it gives rise to a comparatively intense noise source which can greatly increase the boundary-layer noise, in particular for Kramer-type surfaces.

FISI, if present, may either affect instability directly or indirectly. As travelling waves they may become unstable before, or grow faster than, the TSI, in which case the experimentally determined neutral curve would correspond to FISI rather than TSI. Alternatively, they may be present as standing waves and alter the pressure gradient along the surface. This may have a stabilizing or destabilizing effect on TSI, depending on whether the modified pressure gradient is favourable or adverse. In the case under consideration, i.e. compliant surfaces consisting of tensioned membranes, the theoretically most unstable mode of FISI is a first-mode divergence (i.e. the membrane simply swells upward in a single hump). If the compliant surface is assumed to run the entire length of the working section (i.e. 3 m)† it can be shown from equation (21) of Garrad & Carpenter (1982) that the critical velocities are 0.325 m/s and 0.184 m/s for the two-dimensional surfaces corresponding to cases B1-B5 and B36-B42 respectively. In the experiments the surfaces had free streamwise edges and Ellen (1977) has shown that the critical speed for such a surface is 0.5–0.6

† This is a conservative assumption; a shorter compliant surface would have a higher critical velocity.

times that of the corresponding two-dimensional surface. The flow speeds in the experiments were 0.11 m/s and 0.13 m/s for cases B1-B5 and B36-B42 respectively, so it appears that the critical velocity for the FISI may well have been exceeded in the latter case at least.†

7.4. *Theoretical results for Kramer coating*

The present methods are now applied to Kramer-type flexible surfaces. The theoretical model used is described in §3.1 and the estimation of the various mechanical parameters for the coatings is discussed in §3.3. The calculated neutral curves corresponding to TSI for various values of the elastic modulus and for a flow speed of 18 m/s are presented in figure 11.‡ For these calculations it was assumed that the fluid substrate was absent (i.e. $\hat{p}_s = 0$ in (4.12)). The Kramer coating with the best performance corresponds to $E = 0.5$ N mm^{-2}; with $E = 0.4$ N mm^{-2} and 1.0 N mm^{-2} respectively for the other two coatings.

It can be seen from figure 11 that the region of instability becomes progressively smaller as E is reduced. This confirms the result obtained by means of the approximate theory presented in §5, since a reduction in E implies a reduction in spring stiffness K and flexural rigidity B which, in turn, implies a reduction in $C_M c_0^2$, keeping C_M fixed. For the particular case of $Re = 1150$ ($Re_\delta = 4000$) Landahl's (1962) figure 5 can be used to provide values for R_Y corresponding to the values of $\bar{\alpha}$ and $\bar{c}_r$ (i.e. a) on the upper and lower branches of the neutral curve for the rigid surface. In this way (5.6) and (5.8) can be used to show that $|\Delta\bar{c}_i|$ increases as E becomes smaller, and $\Delta\bar{c}_i > 0$ for the lower branch of the neutral curve (i.e. the effect is destabilizing), whereas $\Delta\bar{c}_i < 0$ for the upper branch (i.e. stabilizing). The conclusions based on this approximate analysis are borne out by the results presented in figure 11 at $Re = 1150$.

The results of figure 11 can also be compared with predictions of Benjamin's (1960) theory for non-dissipative flexible surfaces. He showed that, when the surface compliance Z (i.e. the surface deflection due to a pressure wave of unit amplitude) is positive, then the neutral curves are shifted to lower wavenumbers and higher Reynolds number, as shown in figure 4.

By using (3.6) with $C_D = C_T = 0$ it can be readily shown that

$$Z = \frac{w}{p_e}\rho c U'(0) = \frac{\bar{U}'(0)\,\bar{c}}{\bar{\alpha}^2\bar{c}^2 C_M - \bar{\alpha}^4 C_B - C_{KE} + \hat{p}_s}. \tag{7.3}$$

In the present case with no substrate, $\hat{p}_s = 0$. C_M, C_B and C_{KE} all depend on Re, as shown in (6.5), so Z is a function of $\bar{\alpha}$, $\bar{c}$ and Re for a particular coating. In figure 12 the variation of Z is plotted along the upper and lower branches of the neutral curve for a rigid surface. The procedure adopted was to take the values of $\bar{\alpha}$ and $\bar{c}$ which correspond to neutral stability on the rigid wall at a given value of Re. The parameters C_M, C_B and C_{KE} would then be evaluated for the flexible surface in question and the values of Z obtained from (7.3). From figure 12 it can be seen that, in the case of $E = 0.5$ N mm^{-2}, Z becomes significantly non-zero at about $Re = 1600$ and $Re = 800$, respectively, for the upper and lower branches. These values of Re are close to those for which the neutral curve corresponding to $E = 0.5$ N mm^{-2} in

† It is worth noting that MacMichael, Klebanoff & Mease (1980) have shown that FISI in the form of static divergence probably gave rise to spurious drag reductions in some experimental studies of flows over compliant surfaces.

‡ It should be emphasized that, except for the case of $E = 1.0$ N/mm^2, FISI in the form of travelling-wave flutter also occurred.

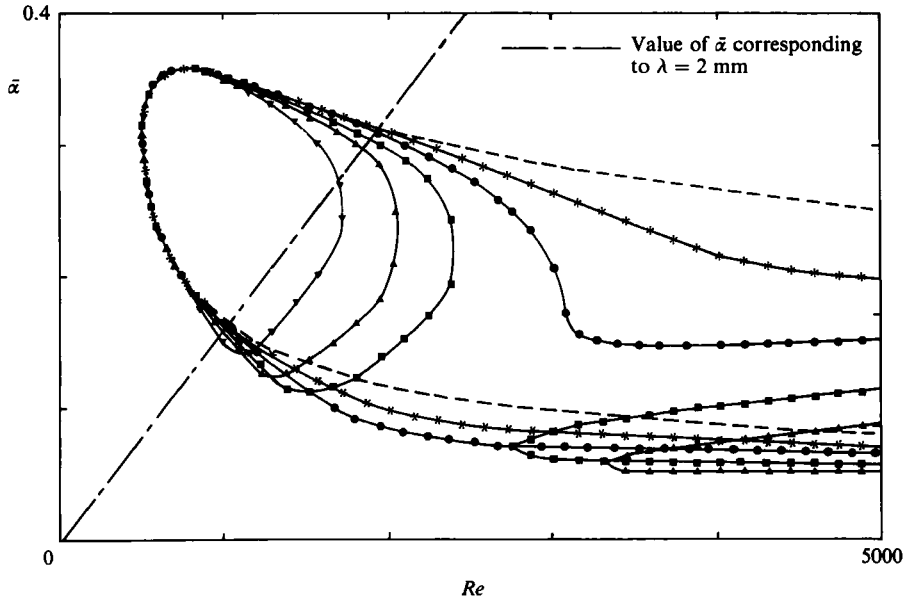

FIGURE 11. The effect of a change in elastic modulus on the neutral curves for Kramer-type compliant surfaces with no substrate fluid and $U_\infty = 18$ m/s: ▼, $E = 0.1$ N mm^{-2}; ▲, 0.2 N mm^{-2}; ■, 0.3 N mm^{-2}; ●, 0.5 N mm^{-2}; *, 1.0 N mm^{-2}; ---, rigid surface.

figure 11 begins to depart from the curve corresponding to the rigid wall. According to Benjamin's theory the neutral curves would be expected to be displaced downward and to the right. This displacement should be greatest where Z is greatest, i.e. at $Re \approx 5500$ on the upper branch and at $Re \approx 2500$ on the lower one. This is much in accordance with what is shown in figure 11. The greatest displacement is observed at around $Re = 2500$. In fact, for values of E less than 0.5 N mm^{-2} the effect is so pronounced that the neutral curve bifurcates into two separate loops. Also shown in figure 12 is the behaviour of Z for a Kramer-type coating with no springy foundation. As might be expected these results show that bending stiffness determines the stability characteristics at the low Reynolds numbers whereas it is the spring stiffness that determines them at the higher Reynolds numbers.

The transitional Reynolds number can be estimated by means of the e^n method of Smith & Gamberoni (1956). With this method it is assumed that the transition point is determined by the relationship

$$\int_{x_i}^{x_{tr}} \frac{\alpha c_i}{c_r}\,dx = n, \tag{7.4}$$

where x_i represents the point of instability and x_{tr} the transition point. Equation (7.4) can be rewritten as

$$\int_{Re_i}^{Re_{tr}} \frac{\bar{\alpha}\bar{c}_i}{\bar{c}_r}\,dRe = 1.481n, \tag{7.5}$$

where Re_i and Re_{tr} are based on the values of δ^* at the points of instability and transition respectively. The integral in (7.5) is evaluated keeping the non-dimensional frequency, $\beta(= \bar{\alpha}\bar{c}_r/Re)$, constant. The value of β giving the lowest value of Re_{tr} is sought. Two values of n were used in the present work, namely 9.5 and 7.35. The former value corresponds approximately to transition on rigid walls and the latter

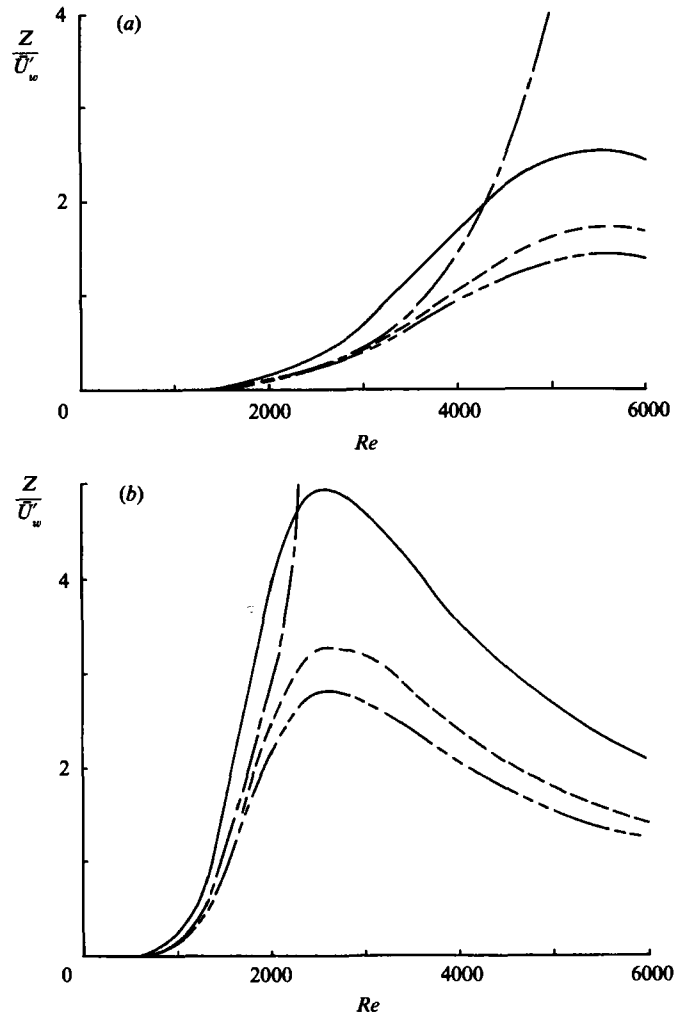

FIGURE 12. The variation of Benjamin's (1960) compliance factor along the neutral curve for some compliant surfaces: ——, $E = 0.3$ N mm^{-2}, and —·—·—, 0.5 N mm^{-2} as in figure 11; — — —, $E = 0.5$ N mm^{-2} and $C_{KE} = 0$; - - - - -, $E = 0.5$ N mm^{-2} as in figure 14 with inviscid substrate fluid. (*a*) Upper branch of neutral curve. (*b*) Lower branch of neutral curve.

value represents approximately the limit of validity for linear theory on rigid walls. The rationale for including calculations based on $n = 7.35$ is that the form of the TSI is likely to be similar on both flexible and rigid surfaces as long as linear theory holds, whereas it cannot be expected that the nonlinear development would be similar for the two types of surface.

The values of transitional Reynolds number† etc. for Kramer's best coating ($E = 0.5$ N mm^{-2}) are given in table 3, together with the corresponding values for a rigid wall. Note that the transitional Reynolds number for the flexible surface is more than twice that for the rigid wall. This suggests that the Kramer coating does have a transition-delaying capability even though the critical Reynolds number is

† It should be emphasized that the transitional Reynolds numbers quoted for the non-dissipative walls in table 3 are based on TSI only.

Coating			Limit of linear growth $n = 7.35$			Transition point $n = 9.5$		
Type	U_∞ (m/s)	ν_s/ν_e	Re	β	λ (mm)	Re	β	λ (mm)
Rigid wall	—	—	2310	42×10^{-6}	3.5	2765	29×10^{-6}	4.9
Kramer coating	18	no substrate	5165	8×10^{-6}	18.1	5845	7×10^{-6}	19.6
Kramer coating†	18	0	5430	7×10^{-6}	21.3	6025	6×10^{-6}	23.3
Kramer coating	18	200	1900	14×10^{-6}	2.0	2105	16×10^{-6}	3.0
Kramer coating	15	10	3915	12×10^{-6}	14.5	4546	10×10^{-6}	16.5
Kramer coating	15	200	2648	18×10^{-6}	10.2	2874	17×10^{-6}	11.2

† Only the results for the TSI mode were used for this calculation.

TABLE 3. Theoretical transitional Reynolds numbers for Kramer coatings. The results given above are for Kramer's coating C ($E = 0.5$ N/mm^2). The values of wavelength correspond to the point of instability.

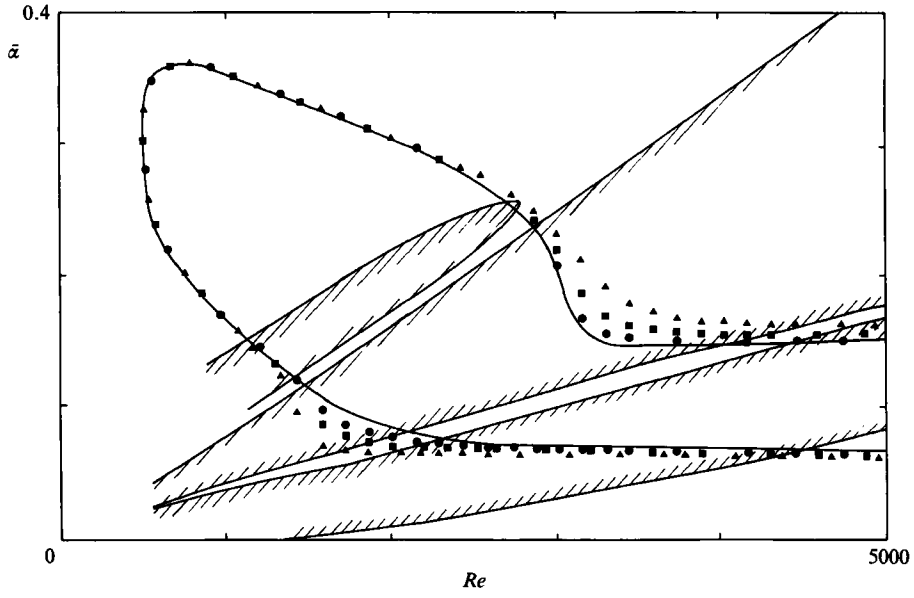

FIGURE 13. The effect of viscoelastic damping on the neutral curves for a Kramer-type compliant surface with no substrate fluid and $E = 0.5$ N/mm^2 and $U_\infty = 18$ m/s: ——, TSI; ////, FISI ($\eta = 0$); ●, $\eta = 0.02$; ■, $\eta = 0.05$; ▲, $\eta = 0.1$ (TSI). The unstable regions for the FISI are denoted by partial shading.

identical with that for the rigid wall. Note also that the most unstable wavelengths involved for the Kramer coating are much longer than the thickness (2 mm) of the elastic plate or diaphragm. This is a fairly important point since the present theory is essentially a long-wave approximation. It becomes invalid when the value of the wavelength approaches the plate thickness. This limiting value of $\bar{\alpha}$ is plotted on figure 11.

The effect of viscoelastic damping on the neutral curves is illustrated in figure 13. For real elastomers E and η vary in a fairly complex way with frequency (e.g. see figure 6). The results in figure 13 are for the simple case of constant E and η. Neutral

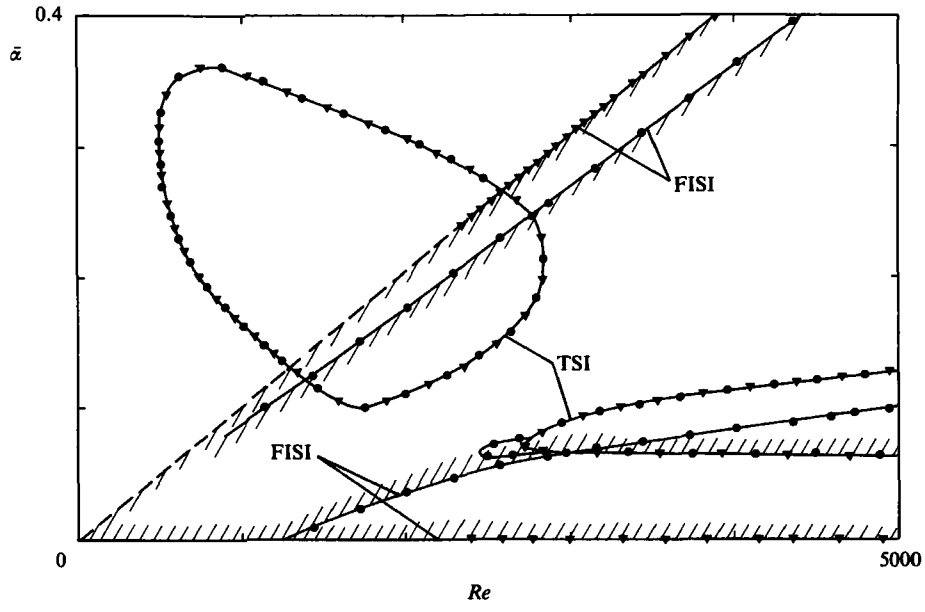

FIGURE 14. Neutral curves for a Kramer-type compliant surface with an inviscid and a slightly viscous fluid substrate, $E = 0.5$ N mm^{-2}, $U_\infty = 18$ m/s and $\eta = 0$: ▼, $\nu_s/\nu_e = 0$; ●, $\nu_s/\nu_e = 1.0$. The unstable regions for the FISI are denoted by partial shading.

curves for both the TSI and FISI are shown in figure 13. It can be seen that viscoelastic damping has a slightly destabilizing effect on the TSI. The stabilizing effect on the FISI (i.e. in the form of travelling waves) is, however, much more pronounced. For even the lightest damping (e.g. $\eta = 0.02$) the FISI disappear completely. The neutral curves for the FISI with $\eta = 0$ form three separate regions of instability which are found within the cross-hatched regions shown in figure 13. The growth rates in the uppermost and lowest regions are very low compared with those in the central region, however. The numerical results shown in figure 13 for the TSI confirm the conclusion reached in §5 on the basis of the simple theory.

The effect of including an inviscid fluid substrate is illustrated in figure 14. The neutral curves for TSI in figure 14 comprise two separate loops as compared with the single loop obtained with no substrate, shown in figures 11 and 13. Thus it can be seen that an inviscid fluid substrate has a stabilizing influence on the TSI in accordance with the conclusion based on the approximate theory presented in §5. Reference to figure 12 shows that the inclusion of an inviscid fluid substrate is broadly similar in effect to a reduction in elastic modulus. Also shown in figure 14 are the neutral curves corresponding to the FISI. These take a completely different form from the TSI ones and, incidentally, are considerably more troublesome to compute. The FISI takes the form of a travelling-wave flutter with a phase speed fairly close to the free-stream velocity, which in turn is fairly close to c_0, the free-wave speed. The FISI were identified by comparing the results of numerically integrating the Orr–Sommerfeld equation with those obtained with the purely inviscid theory. This inviscid theory is described briefly by Carpenter (1984*b*) and will be described in more detail in Part 2.

The neutral curves corresponding to a slightly viscous substrate fluid ($\nu_s/\nu_e = 1$) are also included in figure 14. It will be observed that the region of instability is slightly extended for the TSI and considerably reduced for the FISI. This behaviour

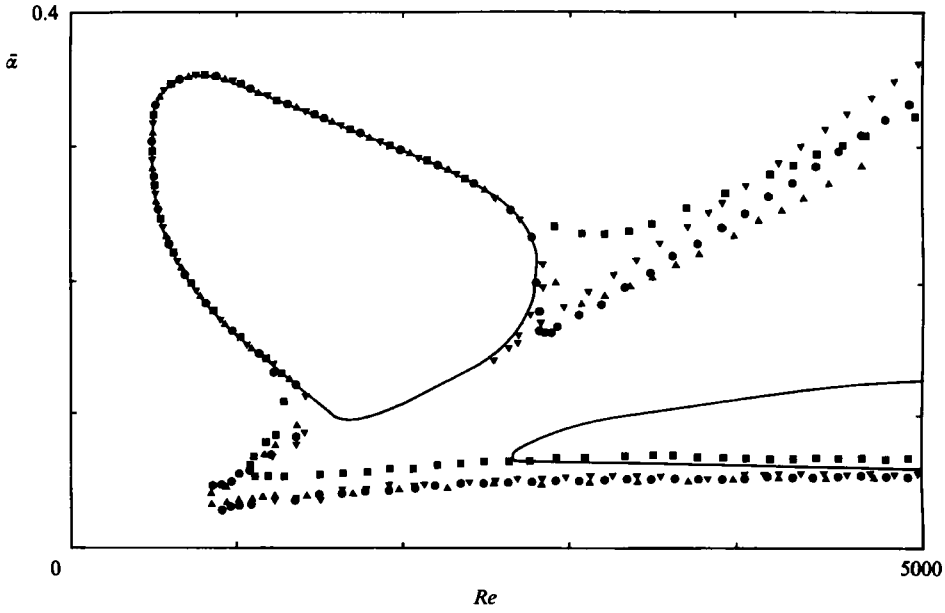

FIGURE 15. The effects of substrate viscosity on the neutral curves for a Kramer-type compliant surface. $E = 0.5$ N mm^{-2} and $U_\infty = 18$ m/s: ——, $\nu_s/\nu_e = 0$; ▼, 50; ●, 100; ▲, 200; ■, 1000.

is consistent with predictions of the simple approximate theory in §5 and with the results of the inviscid theory mentioned above. Great difficulty was experienced in computing neutral curves for substrate viscosities between $\nu_s/\nu_e = 1$ and 50. The difficulty appears to be caused by an interaction between the TSI and FISI modes. The relatively simple numerical methods used for the present work are not suitable for dealing with this more complex situation. More advanced techniques have been developed by Dr M. Gaster and Mr G. J. K. Willis for application to the problem of interacting TSI and FISI modes. Their results have confirmed that the modes interact and that branch points exist in the $(\bar{\alpha}, Re)$-plane. (See Carpenter *et al.* 1983 and Part 3 of the present paper).

The present results, taken together with those of Gaster and Willis, suggest that, as the substrate viscosity is increased from zero, three regimes are encountered. For ν_s/ν_e between zero and approximately unity the TSI and FISI modes do not appear to interact. In this regime the effects of damping are in accordance with the predictions of the approximate theories of §5 and Part 2. Between values of ν_s/ν_e close to unity and less than about 50, the TSI and FISI seem to exist as distinct but interacting modes (see Carpenter *et al.* 1983). There may be two complex eigenvalues $\bar{c}$ with positive (i.e. unstable) imaginary parts for parts of the $(\bar{\alpha}, Re)$-plane. In this regime the viscous damping seems to have a stabilizing effect on the TSI in that the second neutral-stability loop found at $Re \gtrsim 2600$ in figure 14 disappears when ν_s/ν_e exceeds a small value. It was not possible to determine this value at all precisely using the present methods. According to Carpenter *et al.* (1983) the second TSI loop disappeared at $\nu_s/\nu_e \simeq 2.5$ but the value of bending stiffness was slightly different for their calculations. For values of ν_s/ν_e greater than or equal to about 50 the process of coalescence between the two modes appears to be complete. There is now no more than one unstable eigenvalue for each point in the $(\bar{\alpha}, Re)$-plane. In this third regime it is again possible to compute complete neutral curves by means of the present methods; some examples are shown in figure 15.

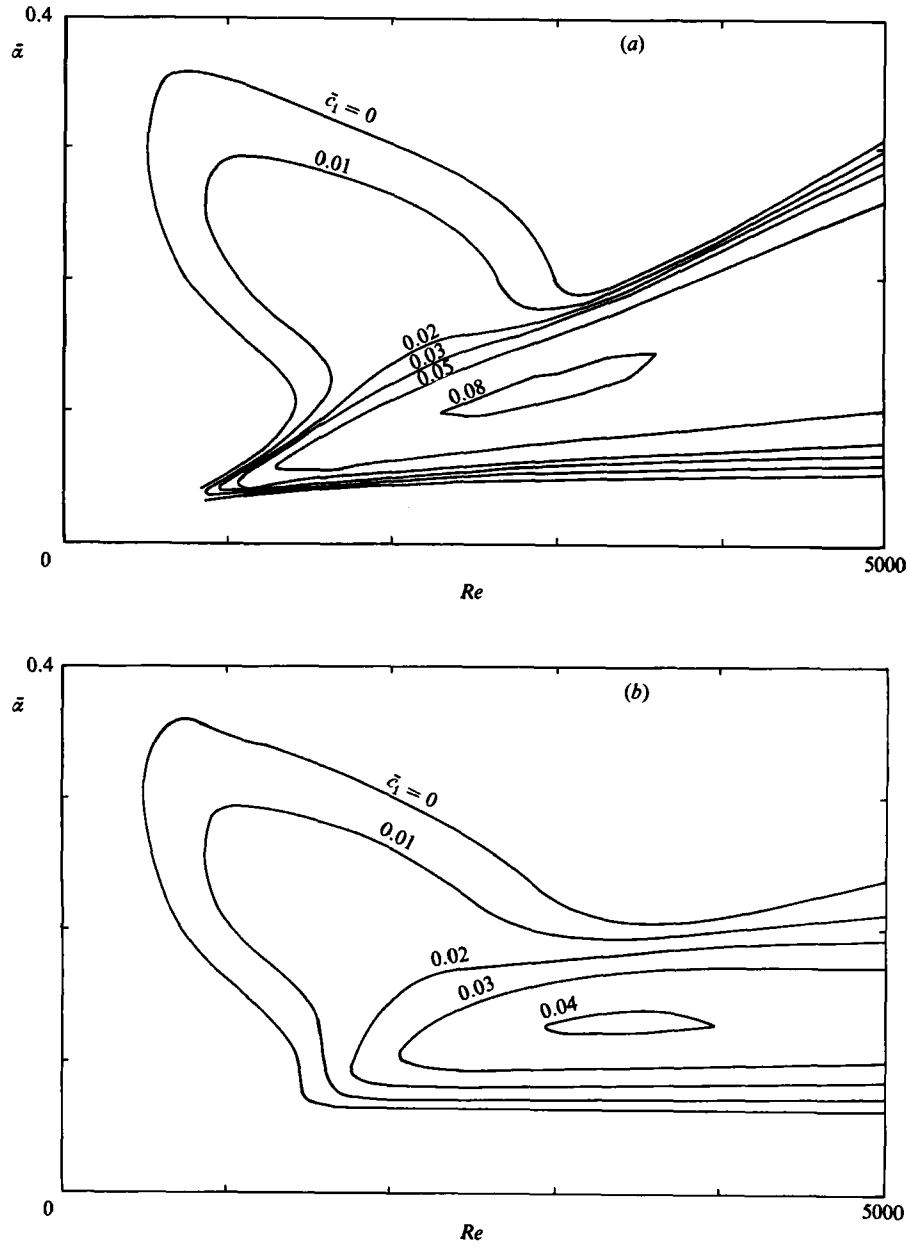

FIGURE 16. Curves for constant $\bar{c}_i$ for Kramer-type compliant surfaces with a viscous fluid surface, $E = 0.5$ N mm^{-2} and $\nu_s/\nu_e = 200$. (*a*) $U_\infty = 18$ m/s. (*b*) $U_\infty = 15$ m/s.

A comparison of the effects of viscoelastic damping, as depicted in figure 13, and of viscous damping, as in figures 14 and 15, shows that for the present case modal interaction only occurs for viscous damping. However, it should not be concluded that modal interaction is only caused by viscous damping. Figure 3 of Carpenter (1984*a*) shows clear signs of modal interaction, induced solely by viscoelastic damping, for a similar compliant coating with $E = 0.3$ MN/m^2 rather than 0.5 MN/m^2.

Curves of constant $\bar{c}_i$ corresponding to $\nu_s/\nu_e = 200$ and $U_\infty = 18$ m/s are presented

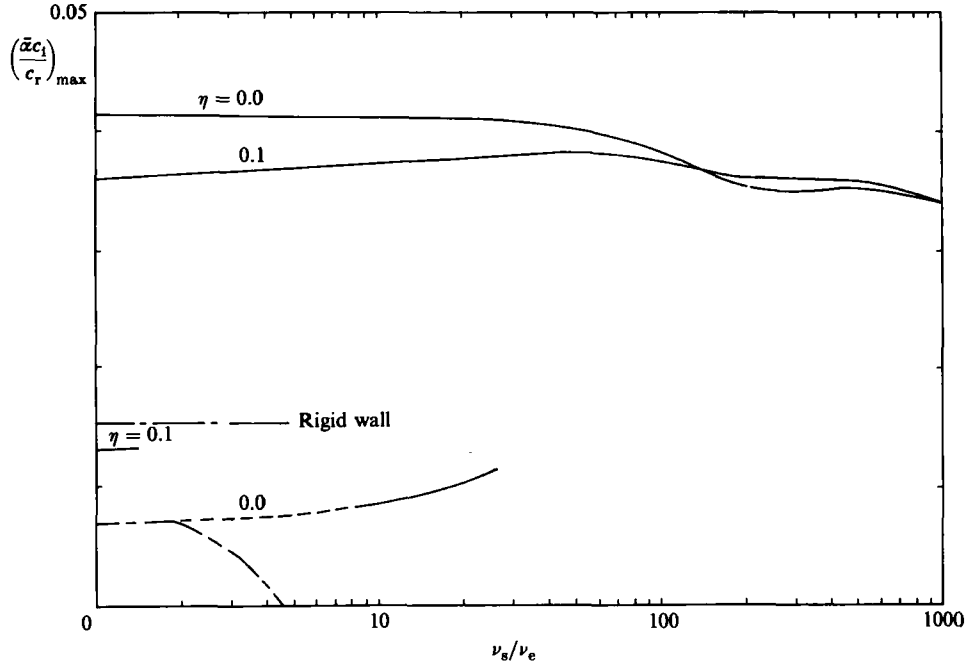

FIGURE 17. The variation of maximum growth rate with substrate viscosity for a Kramer-type compliant surface with and without viscoelastic damping, $E = 0.5$ N/mm^2, $U_\infty = 18$ m/s and $Re = 4735$: ——, FISI and combined instability; —·—, TSI.

in figure 16(*a*). The remnants of the separate TSI and FISI modes can be clearly discerned. In figure 17 the maximum values of $\bar{\alpha}\bar{c}_i/\bar{c}_r$ are plotted against ν_s/ν_e for $\eta = 0.0$ and 0.1: $\bar{\alpha}\bar{c}_i/\bar{c}_r$ is chosen since this quantity provides the best guide to the effect of instability growth on transition (see (7.4)). It can be seen that damping has relatively little effect on the growth rate of the combined FISI/TSI mode. This observation fits in with Landahl's (1962) conclusions concerning the interaction of a Class A (energy falling) and Class B (energy rising) instability. The curve corresponding to the TSI in figure 17 is somewhat speculative. The point on the curve corresponding to $\nu_s/\nu_e = 1.0$ was computed using the present methods. It is also known from the results of Carpenter, Gaster & Willis (1983) that the growth rate falls to zero somewhere between $\nu_s/\nu_e = 1$ and $\nu_s/\nu_e = 5$. Note that a 'fossil' remnant of the TSI exists for low to moderate values of ν_s/ν_e, in that there is a shallow local maximum in $\bar{\alpha}\bar{c}_i/\bar{c}_r$ up to about $\nu_s/\nu_e = 26$. The locus of this local maximum appears to extrapolate back to the value of $(\bar{\alpha}\bar{c}_i/\bar{c}_r)_{max}$ corresponding to the TSI at $\nu_s/\nu_e = 1.0$. It is a feature of the combined FISI/TSI mode, however, not of a separate TSI mode.

The phenomenon of modal interaction between the TSI and FISI bears some similarity to the resonant-surface concept discussed by Benjamin (1960) (according to the classification adopted by Benjamin the TSI would be a Class A wave and the travelling-wave flutter FISI a Class B). The only favourable effect of the interaction in the present case, however, is that viscous damping has a stabilizing effect on the combined mode of instability. On the other hand, it can be seen from figures 16(*a*) and 17 that the growth rates for the combined mode considerably exceed those for the rigid wall. It is not surprising, therefore, that the transitional Reynolds number

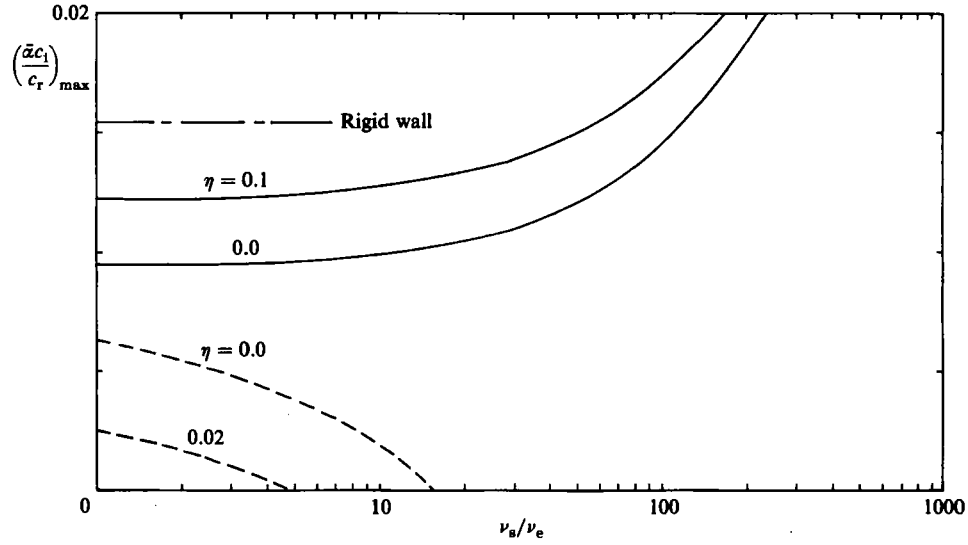

FIGURE 18. The variation of maximum growth rate with substrate viscosity for a Kramer-type compliant surface having various degrees of viscoelastic damping, $E = 0.5$ N mm^{-2}, $U_\infty = 15$ m/s and $Re = 4735$: ——, TSI; -----, FISI.

given in table 3 for $\nu_s/\nu_e = 200$† is substantially lower than that for the rigid wall and very much lower than that for the purely TSI mode with an inviscid substrate fluid. So it appears that transition delay can only be achieved if modal interaction is avoided.

In order to investigate the effects of damping in the absence of modal interaction the calculations were repeated at a free-stream velocity of 15 m/s. Curves of constant $\bar{c}_i$ for a free-stream velocity of 15 m/s and $\nu_s/\nu_e = 200$ are presented in figure 16(*b*). Note that these curves are quite different from the ones shown in figure 16(*a*). There is now no sign of any modal interaction and the TSI and FISI both respond to damping in the manner predicted by the simpler theories (i.e. TSI is destabilized and FISI stabilized). The growth rates, i.e. values of $(\bar{\alpha}\bar{c}_i/\bar{c}_r)_{max}$, for $U_\infty = 15$ m/s are given in figure 18 as functions of ν_s/ν_e for various values of the viscoelastic damping factor η. Note that the FISI is completely eliminated for all but the lowest levels of viscoelastic damping. Note also that for low damping the growth rates are well below the corresponding rigid-wall value. It appears from figure 18 that the stabilizing effects of damping on the FISI are much stronger than its destabilizing effect on the TSI.

Since the viscoelastic damping factor is a material property it may be regarded as a fixed parameter; for Kramer's coatings η is probably of the order of 0.1. Viscous damping, on the other hand, may be regarded as variable. Thus the question arises of how to define the optimum value of ν_s/ν_e for a given level of viscoelastic damping. Two possible definitions are: (i) the value of ν_s/ν_e for which the growth rate of the FISI becomes zero; or (ii) the value at which the growth rates of the FISI and TSI become equal or are closest in value. Clearly these definitions of optimum viscosity would not be applicable when modal interaction occurs; on the other hand, there is

† The growth rate for this case is similar to that for Kramer's optimum value of viscosity.

unlikely to be any prospect of a transition delay when modal interaction occurs. For $U_\infty = 15$ m/s and $\eta = 0.0$ it is apparent from figure 18 that $\nu_s/\nu_e \simeq 16$ is the optimum value according to the first of the above definitions and $\nu_s/\nu_e \lesssim 1.0$ according to the second. For $\eta = 0.1$ the optimum value appears to be $\nu_s/\nu_e \lesssim 1.0$ according to both definitions.

In conclusion, let us return to the question of whether the theoretical results corroborate Kramer's experimental observations. In one important sense Kramer's views have been vindicated. It has been shown (see table 3) that a very considerable transition delay is theoretically possible for Kramer's best coating although not at his top operational speed with his optimum level of viscous damping. Also, when account is taken of the deleterious effect on the FISI of reducing the surface stiffness it seems plausible from the results shown in figure 11 that Kramer's coating C ($E = 0.5$ MN/m^2) should yield better results than either coating B ($E = 1.0$ MN/m^2) or coating D ($E = 0.4$ MN/m^2). It is in the matter of the optimum value of substrate viscosity that theory and experimental observation would appear to differ substantially. The main cause of the discrepancy would appear to be the occurrence of modal interaction. If one were to imagine how the results of figure 17 would appear in the absence of modal interaction, in other words if the growth rates of the TSI and FISI were to behave in a similar fashion to those in figure 18, it seems quite possible that the optimum value of ν_s/ν_e as defined above would be in the region of 100–500. At the same time, bearing in mind that for *TSI alone* the theoretical transitional Reynolds number for an inviscid substrate and $U_\infty = 18$ m/s is well over twice the rigid value (see table 3), there would appear to be ample scope for substantial transition delay in the absence of modal interaction. It would appear, then, that a key question is whether or not modal interaction was likely to have occurred under the conditions of Kramer's tests. Two points should be borne in mind when considering this question. First, the wavelength of the disturbance is relatively small when modal interaction occurs, e.g. according to table 3 for $\nu_s/\nu_e = 200$, $\lambda = 2$–3 mm when $U_\infty = 18$ m/s (modal interaction) but $\lambda = 10$–11 mm when $U_\infty = 15$ m/s (no modal interaction). For wavelengths of the order of the plate thickness (i.e. 2 mm in the case of Kramer's coatings) the present theoretical model is not really valid. For instance, the attenuation of the disturbance as it passes through the thickness of the plate, which is bound to be significant for these short waves, has been neglected in the present theory. One would expect such effects to reduce the growth of the instabilities. The second point to bear in mind is that for the present calculations a flat-plate geometry was assumed, whereas Kramer's models were actually slender bodies of revolution (see figure 1*c*). It is surely rather unreasonable to expect the mechanism of the modal interaction to be unaffected by such relatively large differences in geometry.

8. Conclusions

A theoretical model of a Kramer-type compliant surface has been developed. This model has been used to investigate numerically the hydrodynamic stability of such surfaces. Some other surfaces have also been studied. A simple approximate theory has been developed for predicting the effects of surface properties on the TSI. Under normal circumstances the results of this simple theory are in agreement with the results of the numerical investigation.

The numerical investigation has resulted in the following main conclusions.

(i) There are two main modes of instability, namely Tollmien–Schlichting Instability

(TSI) and Flow-Induced Surface Instability (FISI) in the form of a travelling-wave flutter.

(ii) Damping, both viscous and viscoelastic, normally destabilizes the TSI and stabilizes the FISI. The latter effect appears to be more pronounced.

(iii) Modal interaction and even coalescence between the TSI and FISI may occur when viscous damping is present. Under the conditions investigated in the present paper viscoelastic damping acting alone did not lead to modal interaction. Thus there is a clear difference between the two types of damping.

(iv) Kramer-type coatings are theoretically capable of considerable transition postponement provided modal interaction does not occur.

(v) The opposing effects of damping on the TSI and FISI may lead to optimum values of substrate viscosity.

(vi) The neutral curves obtained experimentally by Babenko *et al.* for flows over tensioned membranes do not agree with those predicted by linear hydrodynamic stability theory.

The authors would like to thank Dr I. Gladwell (Department of Mathematics, University of Manchester) who advised them to use the orthogonalization code SUPORT and passed on to them a copy obtained from its authors. They also wish to acknowledge the valuable information and advice provided by Dr M. Gaster and Mr G. J. K. Willis of NMI Ltd during many helpful discussions. The work described above is part of a research programme at Exeter which is being carried out with the support of Procurement Executive, Ministry of Defence; it was started when one of the authors (A. D. G.) was in receipt of an S.E.R.C. studentship.

REFERENCES

ALEEV, YU. G. 1977 *Nekton*. The Hague: Junk.

ALFREY, T. 1944 Non-homogeneous stresses in viscoelastic media. *Q. Appl. Maths* **2**, 113–119.

AMFILOKHIEV, V. B., DROBLENKOV, V. V. & ZAVORDKHINA, A. S. 1972 Growth of small disturbances in a boundary layer on an elastic surface. [In Russian.] *PMTF-Zh. Prikl. Mekh. i Tekh. Fiz.*, March–April, 137–139.

BABENKO, V. V. 1973*a* Experimental investigation of the hydrodynamic stability for simple flat membrane surfaces. [In Russian.] *Gidromekhanika* **24**, 3–11.

BABENKO, V. V. 1973*b* A method for determining the mechanical properties of flexible coatings. [In Russian.] *Bionika* **7**, 71–79.

BABENKO, V. V., GINTETSKII, N. A. & KOZLOV, L. F. 1969 Preliminary results of an investigation into the elastic properties of the skin of a living dolphin. [In Russian.] *Bionika* **3**, 12–19.

BABENKO, V. V., GINTETSKII, N. A. & KOZLOV, L. F. 1972 A low-turbulence hydrodynamic stand, apparatus and method of investigating the stability of a laminar boundary layer. [In Russian.] *Bionika* **6**, 84–89.

BABENKO, V. V. & KOZLOV, L. F. 1973 Experimental investigation of hydrodynamic stability on rigid and elastic-damping surfaces. [In Russian.] *Izv. Akad. Nauk SSSR, Mekh. Zhidk. i Gaza*, no. 1, 122–127.

BABENKO, V. V., KOZLOV, L. F. & PERSHIN, S. V. 1972 On the variable damping of dolphin skin at various swimming speeds. [In Russian.] *Bionika* **6**, 42–52.

BABENKO, V. V. & SURKINA, P. M. 1969 Some hydrodynamic features of dolphin swimming. [In Russian.] *Bionika* **3**, 19–26.

BARRY, M. D. J. & ROSS, M. A. S. 1970 The flat plate boundary layer. Part 2. The effect of increasing thickness on stability. *J. Fluid Mech.* **43**, 813–818.

BENJAMIN, T. B. 1959 Shearing flow over a wavy boundary. *J. Fluid Mech.* **6**, 161–205.

BENJAMIN, T. B. 1960 Effects of a flexible boundary on hydrodynamic stability. *J. Fluid Mech.* **9**, 513–532.

BENJAMIN, T. B. 1963 The threefold classification of unstable disturbances in flexible surfaces bounding inviscid flows. *J. Fluid Mech.* **16**, 436–450.

BENJAMIN, T. B. 1964 Fluid flow with flexible boundaries. *Proc. 11th Intl Congr. Appl. Maths Munich, Germany* (ed. H. Görtler), pp. 109–128. Springer-Verlag.

BETCHOV, R. 1960 Simplified analysis of boundary-layer oscillations. *J. Ship Res.* **4**, 37–54.

BETCHOV, R. & CRIMINALE, W. O. 1967 *Stability of Parallel Flows.* Academic.

BLICK, E. F., WALTERS, R. R., SMITH, R. & CHU, H. 1969 Compliant coating skin friction experiments. *AIAA Paper* no. 69–169.

BUSHNELL, D. M. & HEFNER, J. N. 1977 Effect of compliant wall motion on turbulent boundary layers. *Phys. Fluids* **20**, S31–S48.

CARPENTER, P. W. 1984*a* The effects of damping on the hydrodynamic stability of flows over Kramer-type compliant surfaces. In *Laminar/Turbulent Boundary Layers* (ed. E. M. Uram & H. E. Weber), pp. 53–59. ASME.

CARPENTER, P. W. 1984*b* The effect of a boundary layer on the hydroelastic instability of infinitely long plates. *J. Sound Vib.* **93**, 461–464.

CARPENTER, P. W. & GARRAD, A. D. 1982 Effect of a viscous fluid substrate on the flow-induced vibrations of a compliant coating. In *Proc. Intl Conf. on Flow Induced Vibrations in Fluid Engineering, Reading, England*, pp. 369–382.

CARPENTER, P. W., GASTER, M. & WILLIS, G. J. K. 1983 A numerical investigation into boundary-layer stability on compliant surfaces. In *Numerical Methods in Laminar and Turbulent Flow* (ed. C. Taylor *et al.*), pp. 166–172. Swansea: Pineridge.

DE LOOF, J. P. 1974 A synthesis on drag reduction experiments at Bertin. From compliant surfaces and gas film to polymers. In *Proc. Int. Conf. on Drag Reduction, Cambridge*, F3-37-52.

DINKELACKER, A. 1977 On the problem of drag reduction by means of compliant walls. *AGARD Rep.* No. 654 (Special Course on Concepts for Drag Reduction), chap. 8, pp. 1–21.

ELLEN, C. H. 1977 The stability of an isolated rectangular surface embedded in uniform subsonic flow. *Trans ASME* E: *J. Appl. Mech.* **44**, 201–206.

FASEL, H. 1980 Recent developments in the numerical solution to the Navier–Stokes equations and hydrodynamic stability problems. In *Computational Fluid Dynamics* (ed. W. Kollmann), pp. 167–280. Hemisphere.

FISCHER, M. C., WEINSTEIN, L. M., BUSHNELL, D. M. & ASH, R. L. 1975 Compliant wall-turbulent skin-friction reduction research. *AIAA Paper* no. 75-833.

FFOWCS WILLIAMS, J. E. 1964 Reynolds stress near a flexible surface responding to unsteady air flow. *Bolt Beranek and Newman Inc., Cambridge, Mass.*, rep. no. 1138.

GARRAD, A. D. 1980 A study of flow over flexible surfaces of simple membrane type. Ph.D. thesis, University of Exeter.

GARRAD, A. D. & CARPENTER, P. W. 1982 A theoretical investigation of flow-induced instabilities in compliant coatings. *J. Sound Vib.* **85**, 483–500.

GASTER, M. 1974 On the effects of boundary-layer growth on flow stability. *J. Fluid Mech.* **66**, 465–480.

GEAR, C. W. 1971 *Numerical Initial Value Problems in Ordinary Differential Equations.* Prentice-Hall.

GERSTING, J. M. 1980 Numerical methods for eigen systems: The Orr–Sommerfeld problem. *Computers & Maths with Applications* **6**, 167–174.

GERSTING, J. M. & JANKOWSKI, D. F. 1972 Numerical methods for Orr–Sommerfeld problems. *Intl J. Numer. Meths Engng* **14**, 195–206.

GROSSKREUTZ, R. 1971 Wechselwirkungen zwischen turbulenten Grenzschichten und weichen Wänden. *MPI für Strömungsforschung und der AVA, Göttingen, Mitt. No.* 53.

GROSSKREUTZ, R. 1975 An attempt to control boundary-layer turbulence with nonisotropic compliant walls. *University Science Journal* (*Dar es Salaam*) **1**, 67–73.

GYORGYFALVY, D. 1967 Possibilities of drag reduction by the use of flexible skin. *J. Aircraft* **4**, 186–192.

HOWE, M. S. 1983 The influence of surface compliance on the production of sound by a turbulent boundary layer. In *Proc. Int. ASME Symp. on Turbulence Induced Vibrations and Noise in Structures, 13–18 November.*

JORDINSON, R. 1970 The flat plate boundary. Part 1. Numerical integration of the Orr–Sommerfeld equation. *J. Fluid Mech.* **43**, 801–811.

KAPLAN, R. E. 1964 The stability of laminar boundary layers in the presence of compliant boundaries. M.I.T., Sc.D. thesis.

KARPLUS, H. B. 1963 Turbulent flow transition near solid and flexible boundaries. *Illinois Inst. Tech. Res. Inst. Rep.* IITRI 1205-4.

KORNECKI, A. 1978 Aeroelastic and hydroelastic instabilities of infinitely long plates. I. *Solid Mechanics Archives* **3**, 381–440.

KOROTKIN, A. I. 1965 The stability of a laminar boundary layer on an elastic surface in an incompressible fluid. [In Russian.] *Izv. Akad. Nauk SSSR, Mekh. Zhid. i Gaza*, no. 3, pp. 39–44.

KRAMER, M. O. 1957 Boundary-layer stabilization by distributed damping. *J. Aero. Sci.* **24**, 459.

KRAMER, M. O. 1960*a* Boundary layer stabilization by distributed damping. *J. Am. Soc. Naval Engrs* **72**, 25–33; *J. Aero/Space Sci.* **27**, 69.

KRAMER, M. O. 1960*b* The dolphins' secret. *New Scientist* **7**, 1118–1120.

KRAMER, M. O. 1962 Boundary layer stabilization by distributed damping. *J. Am. Soc. Naval Engrs* **74**, 341–348.

KRAMER, M. O. 1965 Hydrodynamics of the dolphin. *Adv. in Hydrosci.* **2**, 111–130.

LANDAHL, M. T. 1962 On the stability of a laminar incompressible boundary layer over a flexible surface. *J. Fluid Mech.* **13**, 609–632.

LANDAHL, M. T. & KAPLAN, R. E. 1965 Effect of compliant walls on boundary layer stability and transition. *AGARDograph* 97-1-353.

LIN, C. C. 1945 On the stability of two-dimensional parallel flows, Parts I, II and III. *Q. Appl. Maths* **3**, 117–142, 218–234, 277–301.

MACMICHAEL, J. M., KLEBANOFF, P. S. & MEASE, N. E. 1980 Experimental investigation of drag on a compliant surface. *Prog. Astronautics* **72**, 410–438.

MATTOUT, R. 1972 Réduction de trainée par parois souples. *Bull. Ass. Tech. Maritime et Aéro.* **72**, 207–227.

MEALS, R. 1969 Silicon compounds (silicones). *Kirk-Othmer Encyclopedia of Chemical Technology* **18**, 221–260.

NISEWANGER, C. R. 1964 Flow noise and drag measurements of vehicle with compliant coating. *U.S. Naval Ordnance Test Station, China Lake, California. NAVWEPS Rep.* 8518.

NONWEILER, T. 1961 Qualitative solutions of the stability equation for a boundary layer in contact with various forms of flexible surface. *A.R.C. Rep. No.* 22,670.

OSTROWSKI, A. M. 1960 *Solution of Equations and System of Equations.* Academic.

PAYNE, A. R. 1958 Temperature-frequency relationships of dielectric and mechanical properties of polymers. In *The Rheology of Elastomers* (ed. P. Mason & N. Wookey), pp. 86–112. Pergamon.

PURYEAR, F. W. 1962 Boundary layer control drag reduction by compliant surfaces. *U.S. Dept. of Navy, David Taylor Model Basin. Report* 1668.

RICHARDS, B. 1968 Stability and compliant surfaces. *AGARD-VKI Lecture Series on Mechanics of Boundary Layer Transition*, Lecture Series 3, pt 4.

RITTER, H. & MESSUM, L. T. 1964 Water tunnel measurements of turbulent skin friction on six different compliant surfaces of one foot length. *Admiralty Research Laboratory Report* ARL/G/N9.

RITTER, H. & PORTEOUS, J. S. 1965 Water tunnel measurements of skin friction on a compliant coating. *Admiralty Research Laboratory Report* ARL/N3/G/HY/9/7.

ROSENHEAD, L. 1963 *Laminar Boundary Layers.* Clarendon.

ROSS, J. A., BARNES, F. H., BURNS, J. G. & ROSS, M. A. S. 1970 The flat plate boundary layer. Part 3. Comparison of theory with experiment. *J. Fluid Mech.* **43**, 819–832.

SCHLICHTING, H. 1933 Zur Entstehung der Turbulenz bei der Plattenströmung. *Z. angew. Math. Mech.* **13**, 171–174.

SCHLICHTING, H. 1968 *Boundary Layer Theory*, 6th edn. McGraw-Hill.

SCHUBAUER, G. B. & SKRAMSTAD, H. K. 1948 Laminar boundary layer oscillations and transition on a flat plate. *NACA Rep.* 909.

SCOTT, M. R. & WATTS, H. A. 1975 SUPORT: a computer code for two-point boundary-value problems via ortho-normalization. *Sandia Labs. Report no.* SAND75-0198.

SMITH, A. M. O. & GAMBERONI, H. 1956 Transition, pressure gradient and stability theory. *Douglas Aircraft Co., Long Beach, Calif., Rep.* ES26388.

TOLLMIEN, W. 1929 Über die Entstehung der Turbulenz. *1. Mitt., Nachr. Ges. Wiss. Göttingen, Math. Phys. Klasse*, pp. 21–44.

WALTERS, R. R. & BLICK, E. F. 1968 Turbulent boundary layer characteristics of compliant surfaces. *J. Aircraft* **5**, 11–16.

WORTMANN, F. X. 1953 Eine Method zur Beobachtung und Messung von Wasserströmungen mit Tellur. *Z. angew. Math. Phys.* **5**, 201–206.

WORTMANN, F. X. 1969 Visualization of transition. *J. Fluid Mech.* **38**, 473–480.